CZECH TECHNICAL UNIVERSITY
IN PRAGUE

Faculty of Civil Engineering

Department of Mechanics

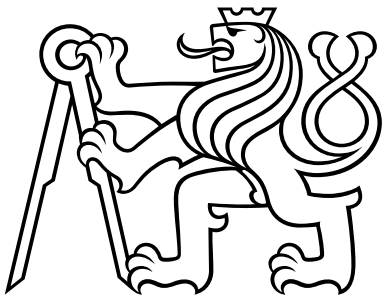

Master's Thesis

Computational modeling of time-dependent behavior of thermoset polymers

Bc. Jan Vozáb

Supervisor: Doc. Ing. Jan Vorel, Ph.D.

Prague, 2019

ČESKÉ VYSOKÉ UČENÍ TECHNICKÉ
V PRAZE

Fakulta stavebního inženýrství

Katedra mechaniky

Diplomová práce

Počítačové modelování časově závislého chování reaktoplastů

Bc. Jan Vozáb

Vedoucí práce: Doc. Ing. Jan Vorel, Ph.D.

Praha, 2019

ZADÁNÍ DIPLOMOVÉ PRÁCE

I. OSOBNÍ A STUDIJNÍ ÚDAJE

Příjmení: **Vozáb** Jméno: **Jan** Osobní číslo: **438389**

Fakulta/ústav: **Fakulta stavební**

Zadávající katedra/ústav: **Katedra mechaniky**

Studijní program: **Stavební inženýrství**

Studijní obor: **Konstrukce a dopravní stavby**

II. ÚDAJE K DIPLOMOVÉ PRÁCI

Název diplomové práce:

Počítačové modelování časově závislého chování reaktoplastů

Název diplomové práce anglicky:

Computational modeling of time-dependent behavior of thermoset polymers

Pokyny pro vypracování:

Seznam doporučené literatury:

Jméno a pracoviště vedoucí(ho) diplomové práce:

doc. Ing. Jan Vorel, Ph.D., katedra mechaniky FSv

Jméno a pracoviště druhé(ho) vedoucí(ho) nebo konzultanta(ky) diplomové práce:

Datum zadání diplomové práce: **26.09.2019** Termín odevzdání diplomové práce: **05.01.2020**

Platnost zadání diplomové práce: _____

doc. Ing. Jan Vorel, Ph.D. podpis vedoucí(ho) práce	podpis vedoucí(ho) ústavu/katedry	prof. Ing. Jiří Máca, CSc. podpis děkana(ky)

III. PŘEVZETÍ ZADÁNÍ

Diplomant bere na vědomí, že je povinen vypracovat diplomovou práci samostatně, bez cizí pomoci, s výjimkou poskytnutých konzultací. Seznam použité literatury, jiných pramenů a jmen konzultantů je třeba uvést v diplomové práci.

.	
Datum převzetí zadání	Podpis studenta

Prohlášení:

Prohlašuji, že jsem svou diplomovou práci vypracoval samostatně a použil jsem pouze podklady (literaturu, projekty, software, atd.) uvedené v přiloženém seznamu.

Nemám závažný důvod proti užití tohoto školního díla ve smyslu § 60 Zákona č. 121/2000 Sb., o právu autorském, o právech souvisejících s právem autorským a o změně některých zákonů (autorský zákon).

V Praze dne 5.1.2020

Jan Vozáb

Název práce:

Počítačové modelování časově závislého chování reaktoplastů

Autor: Jan Vozáb

Obor: Konstrukce a dopravní stavby

Druh práce: Diplomová práce

Vedoucí práce: doc. Ing. Jan Vorel, Ph.D.

Abstrakt:

Mezi materiály, které se začínají v dnešní době více používat patří reaktoplasty. V odvětvích jako je automobilový nebo letecký průmysl jsou reaktoplasty dostatečně vytvrzené, naopak ve stavebnictví jsou často používané vytvrzené nedostatečně, což způsobuje změny vlastností a chování materiálu. Hlavním cílem této práce je vytvoření a implementace numerického modelu, který zachycuje viskoelastické chování tohoto typu materiálu. Model představený v této práci se skládá ze dvou částí. První je elasto-plastický Drucker-Prager model s omezením v tlaku, který popisuje chování materiálu při mechanickém zatěžování. Druhou částí je jeho navázání na model Kelvinova řetězce, který zohledňuje vliv času a zachycuje vliv dotvarování.

Klíčová slova: reaktoplasty, Drucker-Prager, Kelvinův řetězec, dotvarování, metoda konečných prvků

Title:

Computational modeling of time-dependent behavior of thermoset polymers

Author: Jan Vozáb

Abstract:

One of the materials that are becoming more widely used today are thermosets. In sectors such as the automotive or aerospace industries, thermosets are typically sufficiently cured. Conversely, in the construction industry, they are often used when the curing process is not sufficiently completed, which causes changes in the properties and behavior of the material. The main aim of this work is to create and implement a numerical model that captures with sufficient accuracy mechanical response to loading over time. This model consists of two parts. The first is the elasto-plastic model Drucker-Prager with cap, which describes the behavior of the material under mechanical loading. The second part is a Kelvin chain model, which takes into account the influence of time and adds to the behavior the effect of creep.

Key words: thermosetting polymers, Drucker-Prager, Kelvin chain, creep, finite element method

Acknowledgment

I would especially like to thank my supervisor, Doc. Ing. Jan Vorel, Ph.D., for his time and tireless patience to repeat the same things over and over again, without which the work would never have come about. I would also like to thank my girlfriend and family for their language corrections and continued psychological support. I would also like to thank my friends and classmates for their support and ideas in solving problems. This work was supported by Grant No. 19-15666S of the Czech Science Foundation (GAČR).

Contents

List of Figures

Introduction

The history of human creations is interwoven with many different materials. When we look at the beginnings, we find especially those commonly found in nature, such as wood or stone, or even bones. As our development progressed, materials that were more difficult to obtain and process were used. Base metals, alloys, later glass and concrete appeared. With the development of materials, the possibilities of our creations have shifted. The most noticeable development manifested itself with the industrial revolution, when the requirements for material properties, speed and cost of production quickly started to increase. As materials were improved and cheaper, better structures began to be created, leading to additional material requirements. The limit of material options shifts the same as the creation limit. By the end of the first half of the 19th century, human labor was generally more expensive than the materials themselves. This has led to the creation of labor-intensive structures, but very economical in terms of materials. In the second half of the century, the trend began to turn as materials became cheaper and human labor became more expensive, leading to the creation of massive structures. However, with the beginning of the second millennium, higher, longer, more subtle and generally more advanced buildings began to be built. Conventional materials ceased to meet the material properties. Therefore, new types of materials began to develop. Composites are one of these types.

In composite materials, we try to combine desirable properties while eliminating the inadequate. For example, forming materials in which the bearing portion is comprised of carbon or glass fibers held together by polymer matrices. Such materials can be relatively inexpensive, easy to process, and can achieve high strengths. However, their disadvantage is that they tend to be difficult to describe material properties. This is mainly due to the curing of the material but also due to changes in behavior that is caused by environmental changes such as temperature or humidity.

The first chapter is focused on the description of materials, their characteristics and structure. Basic types of materials that are commonly used in civil engineering are described here. Then, thermosets are characterized and major properties are described. Finally, the responses of these materials to loading are depicted.

The second chapter explains the basics of computational modeling. It tries to describe basic parts and problems of element or material simulation, such as boundary conditions, specimen characterization and also numerical model. Then the FEM method is briefly described to explain the numerical implementation of the above mentioned models.

The third chapter focuses on our approach to numerical modeling of materials, which includes elasticity, plasticity and viscosity. There is a Drucker-Prager cap model and then the Kelvin chain is briefly described.

The fourth chapter is devoted to a comparison of the numerical results with experimental data.

1 Materials and their properties

Everything around us is made from matter. Matter is one of the fundamental words, that may be similar in many different languages. According to de Vaan and Watkins [3], it comes from PIE[1] *mater* in Latin, which means "origin, source, mother." The sense was developed and expanded by philosophy by influence of Greek *hylē* in general meaning as "material" used by Aristotle in the philosophical sense. But of all matter surrounding us, only a portion comprises materials, because nowadays they are variously defined. One satisfactory definition is *"all matter used to produce manufactured or consumer goods[12]."* Another definition is *"matter that human beings use and/or process[12]."* In this sense a tree is not material, however, if it is used for wood, it becomes a material. The same applies to all accessible matter: a stone becomes a material when it is used in concrete, and clay becomes a material once it is used for ceramics.[12]

The use and classification of materials depends on their properties. These properties can be grouped into physical, chemical, mechanical, thermal, optical and nuclear and they are tightly connected to the material structure. A schematic framework, that explains the complex relationships in the field of the mechanical behavior of materials, is shown in Fig. 1.1, which contains four principal aspects: properties, performance, structure, and processing. These elements are connected, it means changes in one are inseparably linked to changes in the others. [12]

There are many types of materials depending on their internal structure. Even relatively small changes in the composition of elements can cause significant change in material properties, for example concentration of carbon in steel. High-carbon steel has better resistance to corrosion, but lesser strength. On the other hand low-carbon steel has greater strength. And this is due to a difference of tenths of percent of carbon. Final state of material properties is closely linked to procession, for example cooling rate of steel, or rolling.

1.1 Structure of materials

As we see in Fig.1.1, we can discuss characterization of materials from four perspectives. We can examine structure of material from atomic scale, all the way up to the macro scale. Structure itself is tightly connected to the processing and have direct effect to the material properties and performance. Only solid structure has orderliness of arrangement, gases and liquids are disorderly. But a lot of materials undergo changing chemical state during

[1]Root of Proto-Indo-European languages

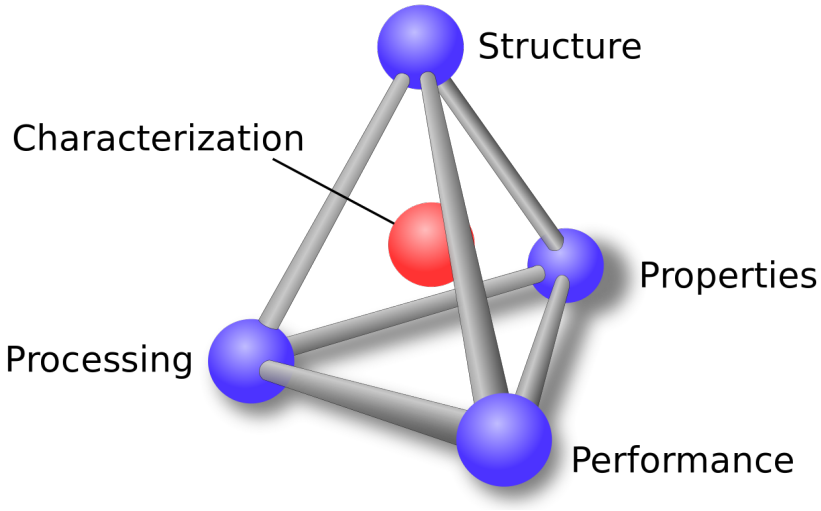

Figure 1.1: Iterative materials tetrahedron applied to mechanical behavior of materials. (After G. Thomas) [1].

procession, for example metals and glass, which can make precise structures thanks to the melting and subsequent cooling. But the cooling rate (processing) influences type of arrangement of atoms which is created. Fast cooling of metal cause creation amorphous structure, as well glass generate internal stress. That will affect directly all properties of the final material. But our interest is focused on polymers, other fundamental materials used in civil engineering are e.g.: metals, ceramics, glasses. [12]

1.1.1 Metals

Metallic structure is composed of closely packed positive ions of metals glued together by electrons. Typically, atoms are packed in the simplest and most compact forms. There are three preferred structures: face-centered cubic, body-centered cubic and hexagonal closest-packed structure, as you can see in Fig. 1.2. Metals are typically shiny, high strength, fusible, ductile, malleable and highly thermal and electrical conductive. [12]

1.1.2 Ceramics

Ceramics can be defined as inorganic non-metallic or carbon man made structure created under high-temperature processing. Such a general definition includes more materials, like glass, glass ceramics, ceramic or carbon layers, or ceramic mono-crystals. The main difference is a fact that glassy structures do not have long range ordering. The structure of ceramics rely on the type of the bond (covalent, ionic or partly metallic), on the processing method and on the sizes of the atoms. Ceramic structure differs from relatively uncomplicated to very complex system. The most typical properties are high melting

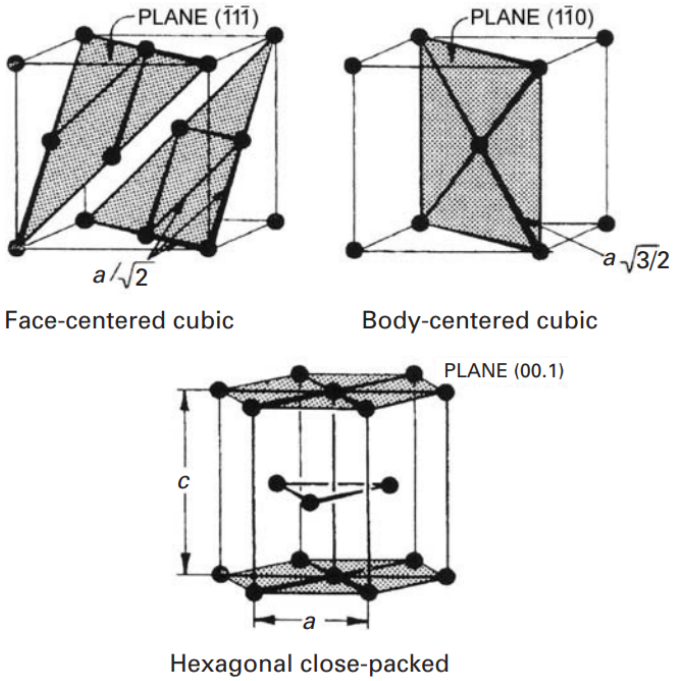

Figure 1.2: Most favored metallic types of bonding. [12].

point, high strength, high durability, low electrical and thermal conductivity and chemical inertness. [12]

1.1.3 Glasses

Glasses differ from ceramics. We cannot find long-range ordering in structure. There is only short-range ordering. Glassy structures are less efficient in arrangement of atoms or molecules, than crystalline structures. If melted material is cooled, contraction occurs. If there is not enough time for crystallization, the material becomes a super-cooled liquid. Contraction follows the liquid line. At material specific *glass transition temperature* the super-cooled liquid is essentially solid. Then material has very high viscosity and it can be called glass. The glassy structures in ceramic can be produce even with relatively low cooling rates. The same mechanisms is valid also for polymeric chains. For metals this is more difficult. Only if material undergoes very high cooling rate, it can create noncrystalline structure. Glasses are typically high strength and fragility.[12]

1.1.4 Polymers

In micro-structure, polymers are more complicated than ceramics and metals. But on the other hand, they are easier and cheaper to process. Generally polymers have lower moduli and strengths. They create giant chains of molecules (macro-molecules), with covalently

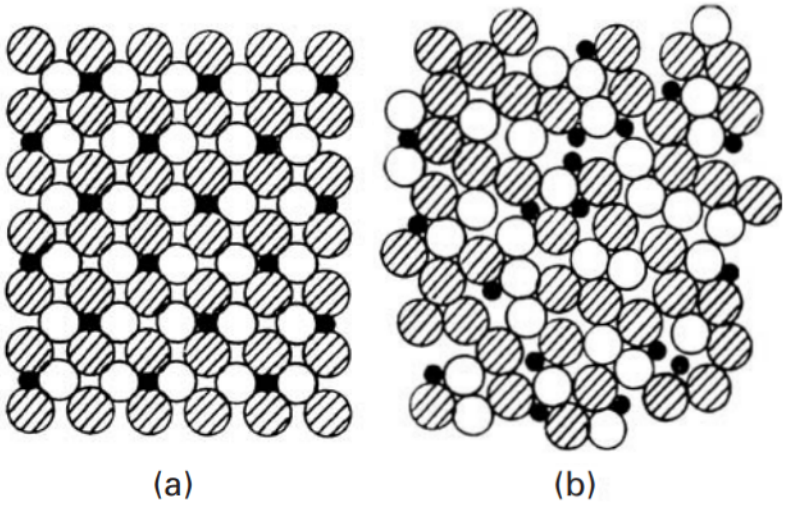

Figure 1.3: Crystalline (a) and glassy (b) structure. [12].

bonded carbon atoms, which form backbone of the chain. The creation of structure is called polymerization. This is process of joining together many monomers (the basic building block of polymers) to form the chains. Polymers are typically poor conductors of electricity and heat, due to the covalent bonds. They are often more chemically inert than metals, mechanical degradation of polymer's properties is caused by exposure of ultra-violent light and by some solvents.[12]

1.1.5 Types of polymers

The main difference in the behavior of polymers comes from their molecular structure and shape, molecular size and weight, and type of bond. You can see different chain configurations in Fig. 1.4. A *linear polymer* is formed of a long chain of atoms with attached side groups. Among these basic polymers we can include polyvinyl chloride or polyethylene. *Branched polymers* consist of branches, which are attached to the main chain. Branching can occur with any types of polymers. *Cross-linked polymers* have molecules of one chain connected with others. That cross-linking of molecular chains create a three-dimensional network. Such structure causes sliding of molecules one by one more difficult. This ensues creation of rigid and strong types of polymers. *Ladder polymers* are formed from two linear polymers linked in a regular manned, which make this structure more rigid than linear polymers.[12]

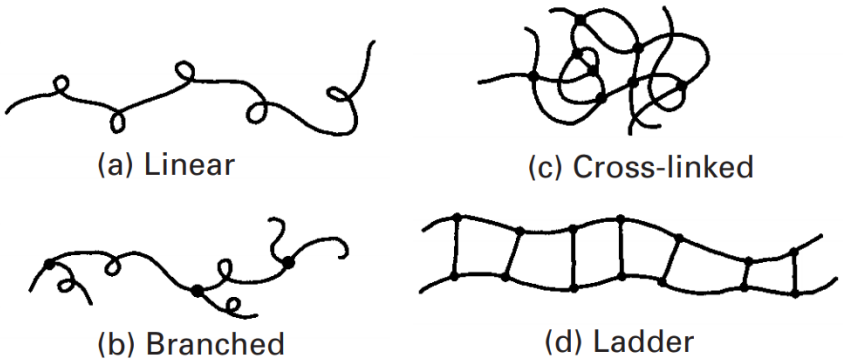

Figure 1.4: Types of polymer molecular chain configurations. [12].

1.2 Thermoset and thermoplastic polymers

Plastic can be classified into two fundamental categories, that are based on their response to temperature: thermoplastic and thermoset. Polymers that soften or even melt upon heating are called thermoplastic. They are formed as linear or branched polymers mostly. On the other hand, when structure is cross-linked, it creates a strong and rigid material. These polymers are called thermosets. Heating leads to degradation without softening or melting. This classification is not restricted just to plastic materials, but can be used on behavior of adhesives, coatings and several other categories. Typical examples of thermoplastic polymers are polypropylene, polyethylene, polystyrene and poly-vinyl chloride. Final shape of thermoplastic polymers is created by heating. This process can be done repeatedly and does not cause any degradation of material properties. As examples of thermosetting polymers we can mention epoxy resins, vinyl-esters, unsaturated polyesters or urea-formaldehyde resin. The difference in behavior of polymers under heating has essential influence on the final shaping of products. Unlike thermoplastic polymers, thermoset polymer network is produced in an irreversible way, that is reason why synthesis of a thermosetting polymer is connected to production of the desired shape of final material. That means, polymerization and final shaping are performed in the same process. [12, 14]

1.2.1 Glass transition temperature

The glass transition temperature T_G has an important influence in polymers behavior, as you can see in Fig.1.5. Below T_G, the modulus of elasticity is higher, behavior is more linear elastic. Above T_G, Young's modulus is considerably lower and material tends to behave as rubbery and viscous. Majority of thermoset polymers are used in environment under their T_G. [14]

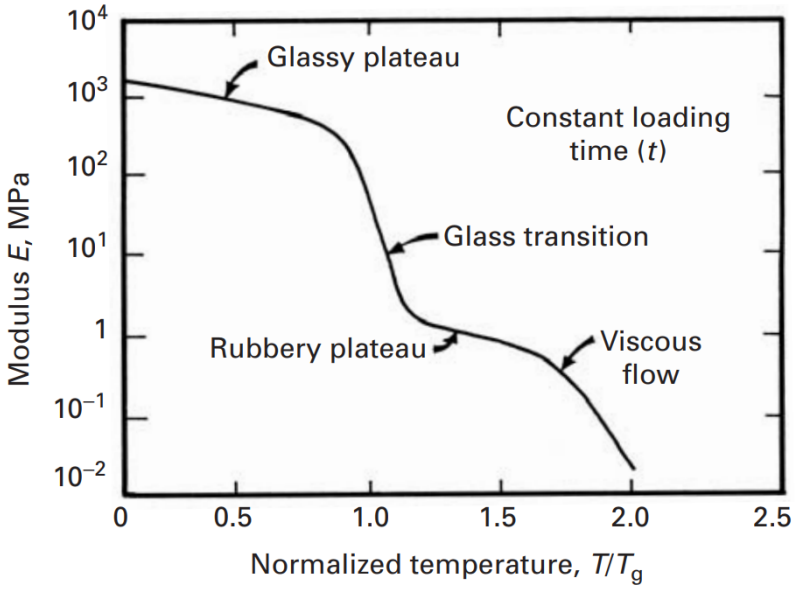

Figure 1.5: Schematic variation in the modulus of elasticity with temperature. [12].

1.3 Primal material responses to loading

Materials under mechanical loading can behave in different ways. State of material is defined by three essential physical variables: *stresses*, which describe internal forces in material, *strains*, which express relative deformation and lastly, *external forces*, which cause both of them. Mechanical response depends on the type of loading, time and other physical and chemical conditions of material, such temperature, humidity, material structure or even history of loading. Generally we divide mechanical behavior into four elemental types:

- elasticity,
- plasticity,
- viscosity,
- fracture.

1.3.1 Elasticity

Elasticity is a part of mechanics, which defines relationship between elastic strain and stress. The elasticity usually describes the material behavior, if the deformation on the body or the structure has not exceed the permissible value. Under that limit material behave elastic, which means that their deformation is reversible when external forces

vanish. Basic definition is generalized Hook's law, which has the form

$$\sigma = D\varepsilon^e, \tag{1.1}$$

where σ means the vector of stresses, D represents the stiffness matrix and ε^e is vector of elastic strains.

1.3.2 Plasticity

Plasticity is ability of the solid material to non-reversibly deform. This type of deformation does not disappear after unloading. This is caused, when internal stresses exceed mechanical yields and limits of material. Then material can response with fracture - breaking of structure, or plasticize - irreversibly changing structure without breaking. For example micro-cracks, which do not change macro-structure, or rearrangement of atoms in metals. [6]

Below the yield limit, material behave still elastic. Together with plasticity it is called elastoplastic (you can see basic examples in Fig. 1.6). There are four classical yield criteria, which define such behavior,

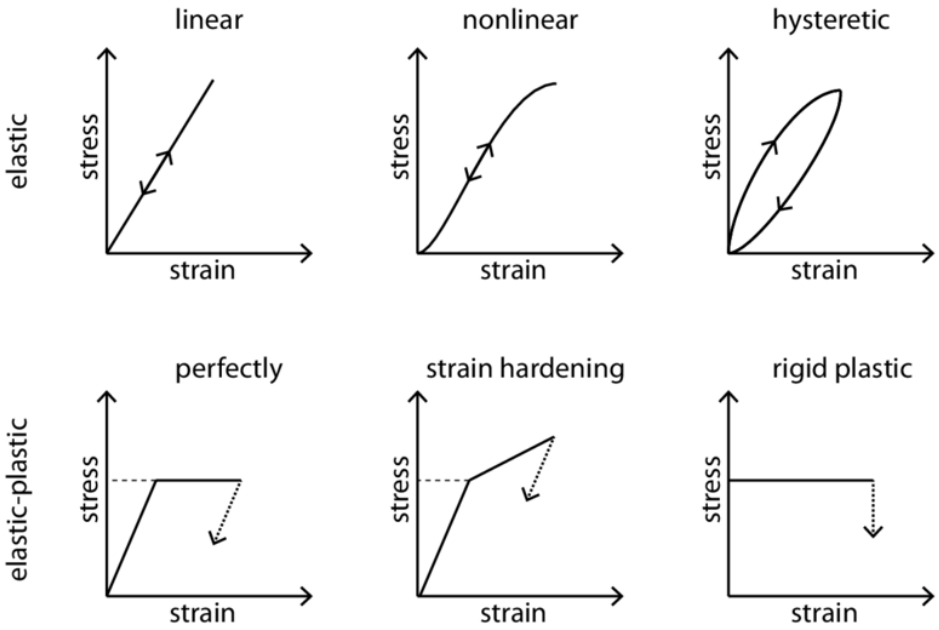

Figure 1.6: Stress-strain relationships for linear and non-linear elasticity as well as plasticity (after Jaeger et al., 2007). Dotted lines denote the unloading curves, dashed lines the yield strength. [19].

- **Tresca** yield criterion (sometimes also known as the maximum shear stress theory), which was published in 1868 to describe plastic yielding in metals. Tresca criterion is described by formula

$$\tfrac{1}{2}\max(|\sigma_1-\sigma_2|,|\sigma_2-\sigma_3|,|\sigma_3-\sigma_1|)=S_{sy}=\tfrac{1}{2}S_y, \tag{1.2}$$

  where S_{sy} represents the yield strength, S_y is the tensile yield strength and σ_1, σ_2 and σ_3 are principal stresses. In the principal stress space it takes the form of a prism.

- Second, **von Mises** yield criterion, is also known as the maximum distortion energy criterion. The plasticity equation has the form

$$J_2=k^2, \tag{1.3}$$

  where J_2 is the second deviatoric stress invariant and k represents the yield stress of the material in pure shear, and it can be obtained from the equation

$$k=\frac{S_y}{\sqrt{3}}. \tag{1.4}$$

  As you can see in Fig. 1.7 and Fig. 1.8, von Mises criterion has in the principal stress space form of cylinder. The main difference between von Mises and Tresca criteria is smoothness of the functions. The von Mises has smooth yield criterion, which simplifies the numerical implementation. Tresca does not have smooth yield, which makes returning more complicated, especially in the turning points.

  Tresca and von Mises are pressure-insensitive. This can be adequate for metals. Other materials, like soils, concrete and rocks, have strength dependence on the yield limit along the hydrostatic axis. This leads to description of pressure-sensitivity.

- **Mohr-Coulomb** yield criterion is in π-plane similar to Tresca yield function, but it is also based on Coulomb's friction law. This criterion presents that plastic yielding of material begins when, on a plane or in the body, the shearing stress τ, and the normal stress σ_n reach the critical combination [6]. General formula describing Mohr-Coulomb criterion is

$$\tau=c-\sigma_n\tan\varphi, \tag{1.5}$$

  where c is a cohesion and φ means the angle of internal friction. In the principal stress plane takes form of hexagonal pyramid aligned with the hydrostatic axis.

- **Drucker-Prager** yield criterion is based on the von Mises criterion and expands it by pressure-sensitivity. It has been proposed in 1952 as a smooth approximation to

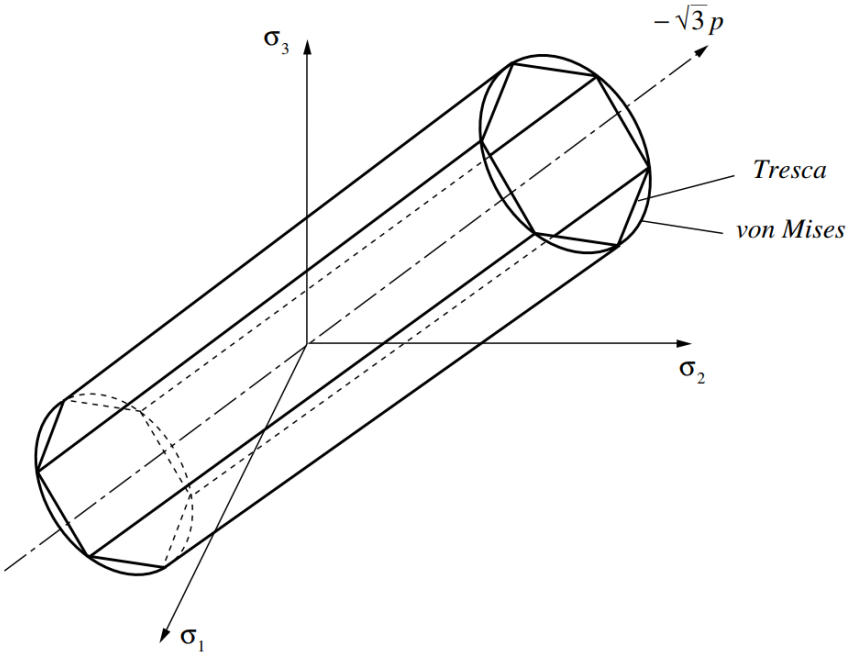

Figure 1.7: Tresca and von Mises yield criterion in the principal stress space. [6]

the Mohr-Coulomb law and assumes the form

$$F(\sigma) = J_2 + (\sigma_m - c\cot\varphi)M_{JP}(\varphi) = 0. \tag{1.6}$$

where σ_m is a effective mean stress, and M_{JP} is a parameter based on the angle of internal friction. In the π-plane it takes the shape like von Mises model, but in the principal stress space it is shaped like cone aligned with the hydrostatic axis. Because of the smoothness and pressure-sensibility, we decided to use this criterion for our numerical description of thermoset polymers. Our approach is described in more details in the third chapter of this thesis.

1.3.3 Fracture

Fracture is a type of material behavior. When the fracture limits are exceeded, the structure is permanently corrupted and softened. This is the main difference between fracture and plasticity. One branch of mechanics is focused on this topic, and it is called fracture mechanics. Main problem is description of the origin and spreading of cracks in the material. [5] However, this is beyond the scope of the thesis and is not described in more details herein.

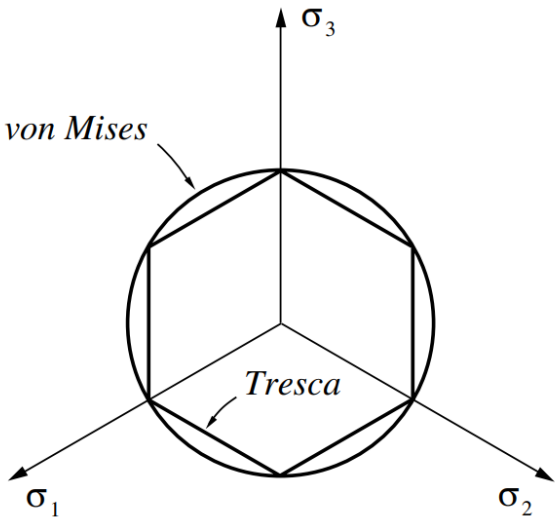

Figure 1.8: Tresca and von Mises yield criterion in the $q\pi$-plane. [6].

1.3.4 Viscosity

Viscosity is an ability of material to permanently deform (plasticize) under yield limit during the time. This ability consists of two effects: creep and relaxation. While creep is tendency of solid material to permanently deform under constant stress, relaxation means decreasing of internal stresses, while strains are constant.

When a material is exhibiting both the elastic and viscous behaviors, it is called viscoelastic. The rheological models[2] are used to describe this general material behavior by combining elements which characterize elastic and viscous performance. In Fig. 1.13 you can see three basic approaches. The first one is Maxwell model, the second is Kelvin-Voigt and the third is their combination. In our approach we chose Kelvin-Voigt chain, because it is typically used to characterize creep behavior of polymers. However, keep in mind that this model is less accurate with regards to relaxation.

[2]Combinations of elements, where each element represent some mechanical behavior - elastic, plastic and viscous element

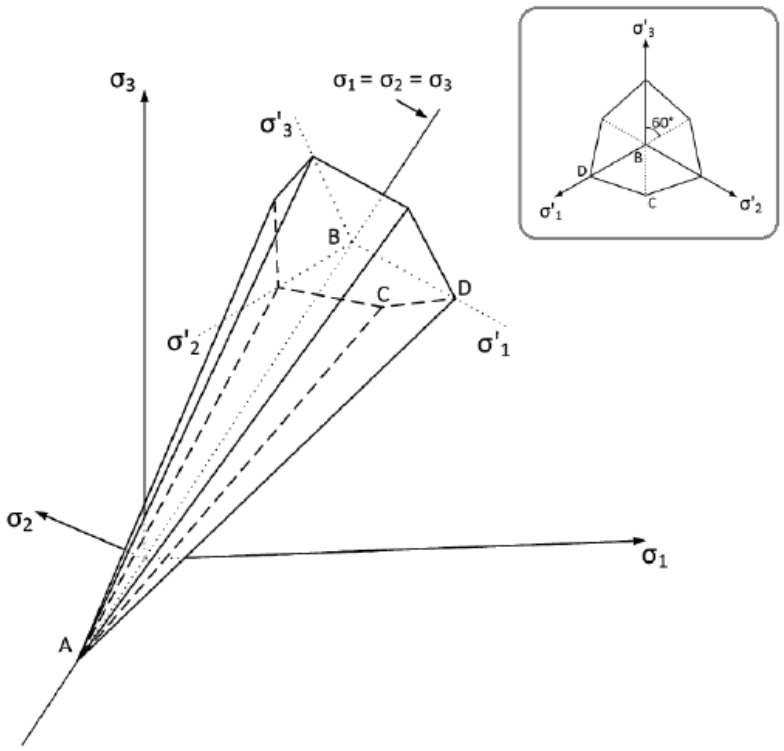

Figure 1.9: Mohr-Coulomb yield criterion in the principal stress space. [11].

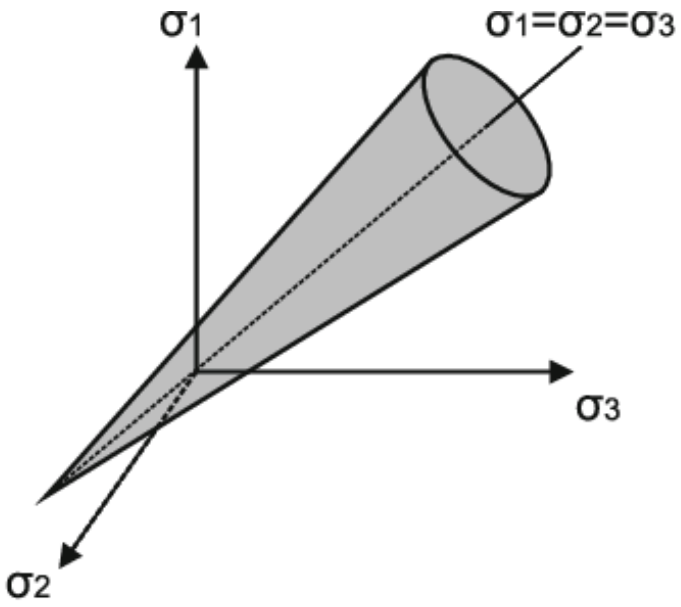

Figure 1.10: Drucker-Prager in the principal stress space. [13].

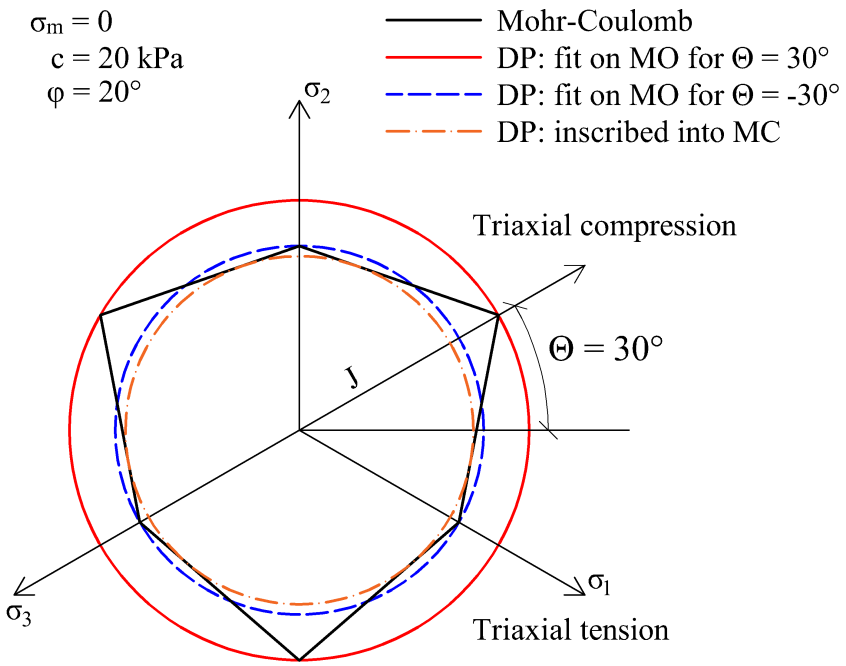

Figure 1.11: Drucker-Prager and Mohr-Coulomb yield criterion in π-plane. [17, 21].

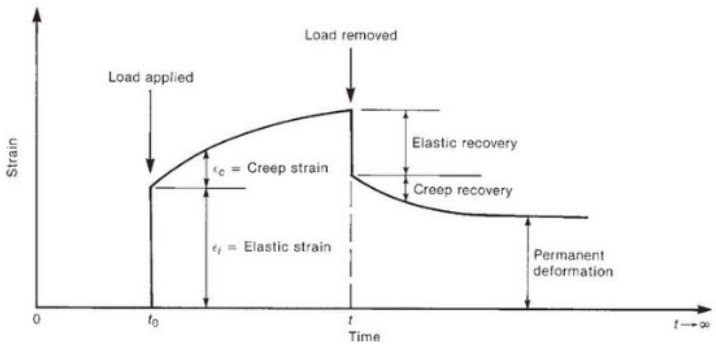

Figure 1.12: Creep Strains due to Loading at time, t0 and unloading at time t. [2].

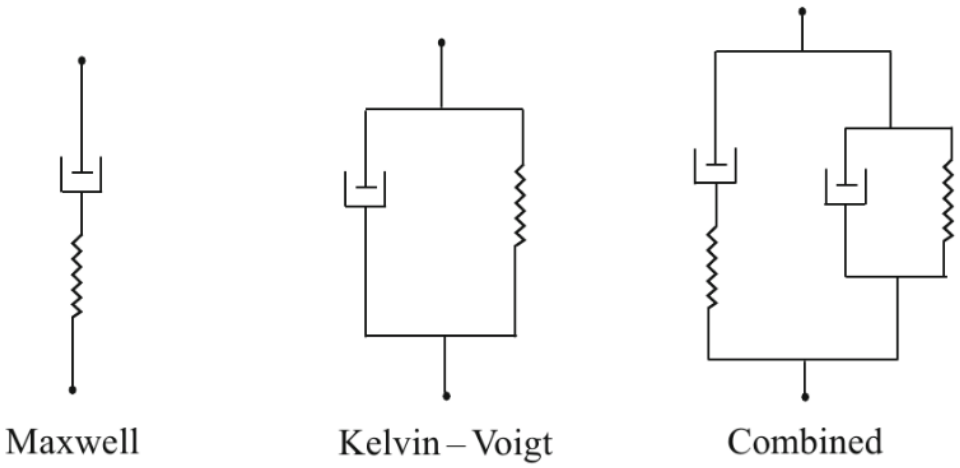

Figure 1.13: Basic reological models for viscoelasticity. [4].

2 Computational modeling

In the previous part we discussed materials and their properties. This chapter is focused more on mathematical description of real-world material behavior. When there is some element, that is made of some material, we can imagine it in the idle state. Newton's First law of motion says that it will remain at rest unless acted upon by force. If we apply load on the element, it will deform. How much, is based on the Newton's Second and Third law. There is always equality between external and internal forces, which causes deformation of material.

If we want to understand how and why material responses, we need theoretical background, like characterization of material and basic responses of materials to loading, both implied in chapter 1. This information will answer the main questions: how and why materials behave as they do. To verify theoretical background we need to test material and measure its real responses. For example to test concrete beam in compression, when we record external forces and deformation of material. The last part of verification is simulation of real testing. It is based on our theoretical background with boundary conditions of real testing. If results of simulation correspond to real measurements, theoretical background is assumed to be correct.

In general, numerical modeling itself can be roughly split into these parts: boundary conditions and material model.

Boundary conditions are constraints necessary for the solution of a boundary value problem which characterizes a vast amount of phenomena and applications. On the other hand, when real element/structure is loaded, deformation of material happens on all structural levels. Therefore, for the numerical simulation a sufficiently accurate model has to be defined to capture the important features of real specimen/structure.

2.1 Numerical model of material

To characterize real material behavior different mathematical models have been created [14]. Complexity of numerical model can vary a lot, from simple Hooke's law for elementary elastic material, to complex microplane models of concrete.

Since the main topic of this thesis are thermoset polymers, we can focus on the modeling of type of materials. Level of complexity of this material can be split into three levels (inspired by[14, 21]).

- *First level* of complexity, where equations describing behavior of material, take into account only two variables: the stress σ and the strain ε:

$$f(\sigma, \varepsilon) = 0. \tag{2.1}$$

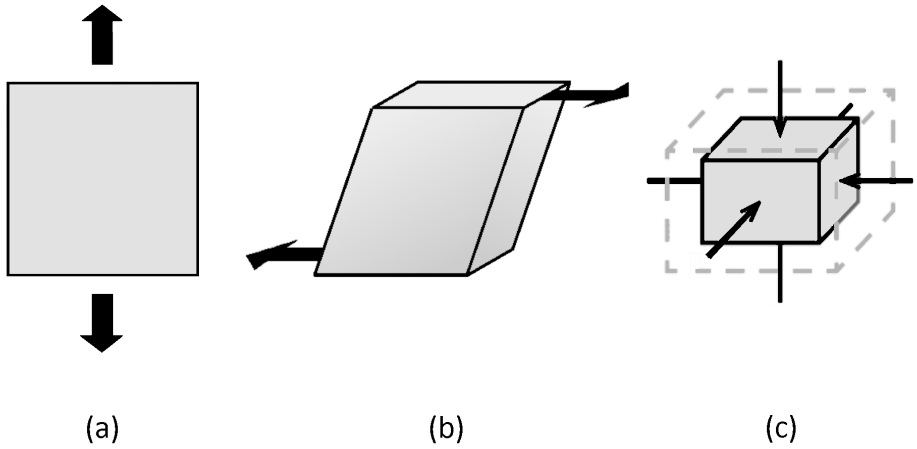

Figure 2.1: Mechanical tests used for determination a) E; b) G; c) K. [14].

This limits describe mechanical simulation for relatively sharp intervals of time and temperature. It can be considered sufficient for a description of material behavior at low strains. For the isotropic material, moduli are defined by the following equations:

$$E = 3K(1-2\nu); \quad G = \frac{3}{2}\frac{(1-2\nu)}{(1+\nu)}; \quad K = \frac{E}{2(1+\nu)}, \tag{2.2}$$

where E is the elastic (Young) modulus, G means the shear (Coulomb) modulus, K represent the bulk modulus, and ν is Poisson's ratio. Modulus E can be obtained from an uniaxial tensile test ($E = \sigma/\varepsilon$), or an uniaxial compression test, or the flexural test; G can be determined from a shear test $G = s/\gamma$, where s is the shear stress and γ is the shear strain; K can be determined from a test of compressibility,

$$K = \left(\frac{1}{V}\frac{dV}{dp}\right)^{-1}, \tag{2.3}$$

where V is the volume and p is the hydrostatic pressure; and ν can be figured out from two independently determined values of modulus, or from a tensile test using a bidimensional extensometer.

- *Second level*, where the constitutive equations should involve two (or more) additional variables. For example:

$$f(\sigma, \varepsilon, \dot{\varepsilon}, T, t, c, \Theta) = 0, \tag{2.4}$$

where $\dot{\varepsilon}$ is the strain rate, T means the temperature, t represents time , c is the

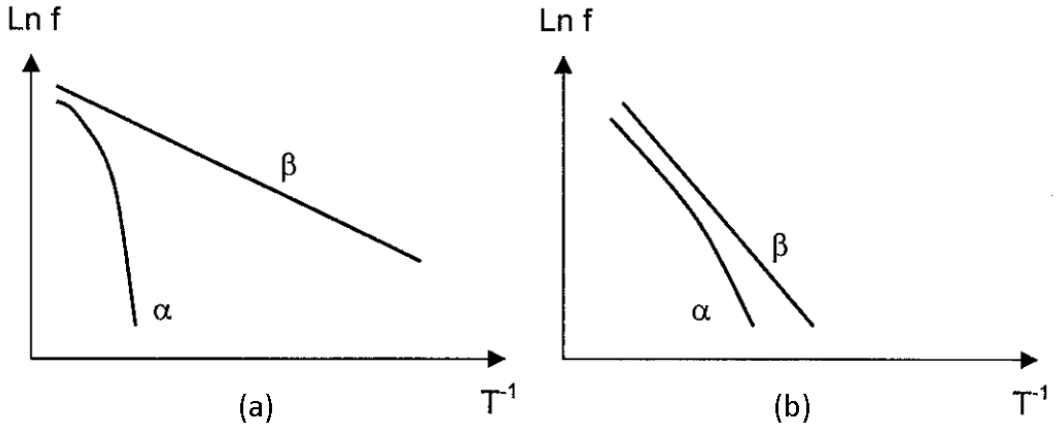

Figure 2.2: Shape of relaxation maps: dependence of ln f (frequency) on reciprocal temperature for coordinates of transitions α, β: (a) - polymers having their α and β transitions well separated; (b) - polymers with close α and β transitions. Inspired by [14].

moisture content and Θ stands for the mechanical dilatation. These new variables are necessary for, e.g., addition of viscoelastic behavior into the material model. This behavior is linked to the molecular motions, which are important in the glassy domain (in Fig. 2.2 between boundaries α and β). They are also affected by the behavior in the glass transition region (around boundary α). High influence on the behavior has also thermo-mechanical history due to a physical aging of the material. The relationships that describe the effects of $\dot{\varepsilon}$, $\dot{\sigma}$, T, t, c and Θ on the previously defined elastic properties are also needed if the extensive model is adopted.

In the literature three major experimental methods for mechanical characterization in this region can be found. They correspond to particular solutions of the material's state equation:

- Static tests: $\varepsilon = \varepsilon_0 = constant$ for relaxation, or $\sigma = \sigma_0 = constant$ for creep.
- Monotonous tests with loading rate $\dot{\varepsilon}$, or $\dot{\sigma} = constant$ (for example tensile tests):
  $\dot{\varepsilon} = \frac{1}{l}\frac{dl}{dt}$.
- Dynamic tests: $\varepsilon = \varepsilon_0 \sin(\omega t)$, or $\sigma = \sigma_0 \sin(\omega t)$.

Polymers are generally assumed to obey the Boltzmann superposition principle in the region of small strains. When are there changes of loading conditions, the effects of these changes are additive when the corresponding responses are considered at equivalent times. For example, if different stresses σ_0, σ_1, σ_2,...σ_i are applied at different times 0, t_1, t_2,...t_i, respectively, the final strain is

$$\varepsilon(t) = J(t)\sigma_0 + J(t-t_1)\sigma_1 + J(t-t_2)\sigma_2 + \cdots + J(t-t_i)\sigma_i \tag{2.5}$$

where $J(t)$ is the time-dependent creep compliance.

In the same manner, if different strains ε_0, ε_1, ε_2,...ε_i are applied at times 0, t_1, t_2,...t_i, the final stress is

$$\sigma(t) = E(t)\varepsilon_0 + E(t-t_1)\varepsilon_1 + E(t-t_2)\varepsilon_2 + \cdots + E(t-t_i)\varepsilon_i \tag{2.6}$$

where $E(t)$ is the time-dependent relaxation modulus. It is generally effective to use dynamic tests to obtain $J(\omega)$ or $E(\omega)$, and then with using mathematical transformations determine $J(t)$ or $E(t)$.

Ordinary, polymers also obey a time-temperature superposition principle [14]:

$$P_r(t,T) = P_r\left(\frac{t}{a_T}, T_r\right), \tag{2.7}$$

where P_r is function of T_r and a_T. In Eq.(2.7), T_r is a reference temperature and a_T is a thermal shift factor that depends on temperature, humidity and mechanical dilatation. Polymers are interesting in fact that $a_T = f(T, c, \Theta)$ takes different mathematical forms below and above glass transition temperature T_g.

2.2 Finite element method

To solve the boundary value problem, we subdividing all systems into finite number of their individual components or elements: These elements have well understand behavior, and with their help we rebuild of the original system from such components. Then we create model that can response and behave like complete system. Such complex model have to satisfy three essential parts described above [22].

In that purpose finite element method was invented. Its foundations can be traced back to the early 1940s. Research was caused by needs of solving complex elasticity and structural analysis tasks in civil and aerospace engineering [10]. Now it is used to solve problems in areas like fields of structural analysis, fluid flow, mass transport, heat transfer or electromagnetic potential. It is used to compute discrete[3] systems, but with the help of discretization and approximation we can solve continuous[4] systems.

[3]Model obtained using a finite number of well-defined components.

[4]Subdivisions of systems would continue infinitesimally, which is technically impossible. Exact solution of models of continuous systems can be solved only by mathematical manipulation.

2.2 Finite element method

Because this thesis is focused on numerical mechanics, we can use basic example of linear elasticity to describe basics of finite element method (FEM). Assuming linear elastic behavior of the element, the characteristic relationship will always have the form

$$q = Ku + f, \tag{2.8}$$

where q is vector of all the nodes of the element, K represents *stiffness matrix* for the element, u means nodal displacement and lastly, f is vector the nodal forces required to balance any concentrated or distributed loads acting on the element [22]. This equality must be applied on every point of every element on the entire model. Initial imbalance of the system is caused by non-zero external load and boundary conditions. Calculation of this system of equations leads to creating balance by solving the displacements of the individual nodes. System of equations is presented by

$$Ku + f = 0. \tag{2.9}$$

Creating FEM system for the calculation of our representative tasks is not part of the thesis. We used MARS Finite element solver [9]. It is robust and powerful solver for simulating the mechanical response of structural systems. It uses explicit time integration scheme for solving the equation of motion of large systems. For results the type of elements, which create mesh, is important. We used single or eight integration points hexahedral elements. Flanagan-Belytschko Hourglass Formulation uses reduced 1 integration point with hourglass control. These elements have worst accuracy, but major advantage is speed of computation. So we used them for testing of simulation. Hexahedral elements with 8 integration points are more complex and results they give are more precise. Calculation is more complicated and more time-consuming. We used hexahedral elements with 8IPs for more precise simulation after calibration.

3 Numerical model

In the previous chapter, we described basics of numerical modeling. What are the essential problems that we need to take into account. This chapter is focused on one of these sections, namely numerical model of the material. In my bachelor thesis [21], we implemented standard Drucker-Prager model with hardening. In this thesis, we decided to use more complex model for greater accuracy. We use Drucker-Prager model, but we added compressive cap. The second part of this chapter is formulation of Kelvin chain and its connection to Drucker-Prager model with cap. This connection help us to simulate viscous behavior of material. These models are implemented in MARS Finite element solver [9] used for all numerical simulations presented herein. The comparison between the experimental data taken from literature [20] and numerical results is presented in the following chapter.

3.1 Drucker-prager model of plasticity

Drucker-Prager model of plasticity can be seen as the extension of the von Mises model and enhances it by including mean stress into the yield surface equation. We also implemented cap in hydrostatic compression. As already mentioned, the definition and the calculation of Drucker-Prager model in this thesis is based on [17].

3.1.1 Drucker-Prager with cap yield surface

Drucker-Prager with cap (DPC) yield criterion describes the limit of elastic behavior. Criterion have the form

$$F(\sigma) = J^2 - \left[(\sigma_m - c(E_d^{pl})\cot\varphi(E_d^{pl}))M_{JP}(\varphi(E_d^{pl}))\right]^2 F_c^c(\sigma_m, X, L) = 0, \tag{3.1}$$

where J is the second invariant of the deviatoric stress, σ_m is the mean stress. J, respectively σ_m can be obtained from

$$J = \sqrt{\frac{1}{6}\left[(\sigma_{11}-\sigma_{22})^2 + (\sigma_{11}-\sigma_{33})^2 + (\sigma_{22}-\sigma_{33})^2\right] + \tau_{12}^2 + \tau_{13}^2 + \tau_{23}^2}, \tag{3.2}$$

$$\sigma_m = \frac{\sigma_{11}+\sigma_{22}+\sigma_{33}}{3}, \tag{3.3}$$

and M_{JP} is used for approximation to the Mohr-Coulomb model. This can be done with three different approaches dependent on desired approximation. Three different Drucker-Prager cones are in Fig. 1.11. The first one, red circle, touches Mohr-Coulomb yield

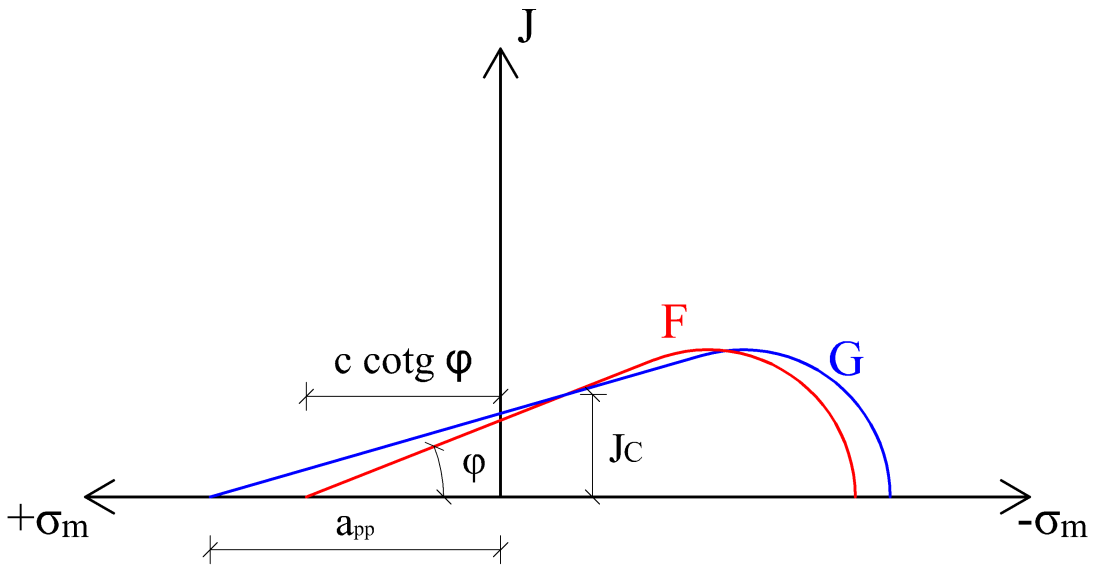

Figure 3.1: Drucker-Prager with cap yield criterion in meridian plane: F is yield function; G means plastic potential function.

criterion at $\theta = 30°$ (triaxial compression) with M_{JP} defined as

$$M_{JP}^{\theta=30°} = \frac{2\sqrt{3}\sin\varphi}{3-\sin\varphi}, \tag{3.4}$$

where φ is the angle of internal friction. The second, blue circle, matched the Mohr-Coulomb model at $\theta = -30°$ (triaxial tension), can be obtained as

$$M_{JP}^{\theta=-30°} = \frac{2\sqrt{3}\sin\varphi}{3+\sin\varphi}, \tag{3.5}$$

and the last, the green circle, is inscribed, and can be determined by

$$M_{JP}^{ins} = \frac{\sin(\varphi)}{\cos(\theta)^{ins} - \frac{\sin(\theta^{ins})\sin(\varphi)}{\sqrt{3}}}, \tag{3.6}$$

$$\theta^{ins} = \arctan\frac{\sin\varphi}{\sqrt{3}}. \tag{3.7}$$

The Drucker-Prager model is not defined just by the yield function F but also G, which is the plastic potential function, see Fig. 3.1. G defines vector of return to the yield of plasticity, when its overpassed, and can be written in the form

$$G = J^2 - \left[(\sigma_m - a_{pp})M_{JP}^{PP}\right]^2 F_c^c, \tag{3.8}$$

where a_{pp} follows from Fig. 3.1. When matching Eqs. (3.1) and (3.8) for the current value of stress σ, result has the form

$$a_{pp} = -\sigma_m^c + (\sigma_m^c - c\cot\varphi)\frac{M_{JP}}{M_{JP}^{PP}} \tag{3.9}$$

where M_{JP}^{PP} is the gradient of the plastic potential function in $J - \sigma_m$ space (Fig 3.1). When functions of plastic potential and yield function $M_{JP}^{PP} = M_{JP}$, Drucker-Prager model becomes associated. M_{JP}^{PP} can be referred as the angle of dilatation ψ, and can be substituted for φ in Equations (3.4)-(3.7).

3.1.2 Hardening and softening of material

In Drucker-Prager model the hardening/softening of material is implemented. We choose multi-linear form of the hardening/softening law for the cohesion c and the angle of internal friction φ, as shown in Fig. 3.2, where the dependence of c and φ on the deviatoric plastic strain E_d^{pl} can be seen.

Multi-linear formulation assumes that if n^{th} interval in Fig. 3.2 is active, then the current strenght parameters can be determined by

$$c = c^{n-1} + h_c^n \left(E_d^{pl} - (E_d^{pl})^{n-1}\right), \tag{3.10}$$

$$\varphi = \varphi^{n-1} + h_\varphi^n \left(E_d^{pl} - (E_d^{pl})^{n-1}\right), \tag{3.11}$$

where h_c^n and h_φ^n are the hardening/softening moduli for c and φ and can be written in the form

$$h_c^n = \frac{c^n - c^{n-1}}{(E_d^{pl})^n - (E_d^{pl})^{n-1}}, \tag{3.12}$$

$$\varphi_c^n = \frac{\varphi^n - \varphi^{n-1}}{(E_d^{pl})^n - (E_d^{pl})^{n-1}}. \tag{3.13}$$

Following [17], the hardening modulus can be determined by

$$H = \left(-\frac{\partial F}{\partial \kappa}\right)^T \frac{\partial \kappa}{\partial \lambda}, \tag{3.14}$$

where κ is hardening/softening parameter (in our case E_d^{pl}). Referring to Fig. 3.2 and using Eq. (3.14) the hardening/softening modulus H assumes the form

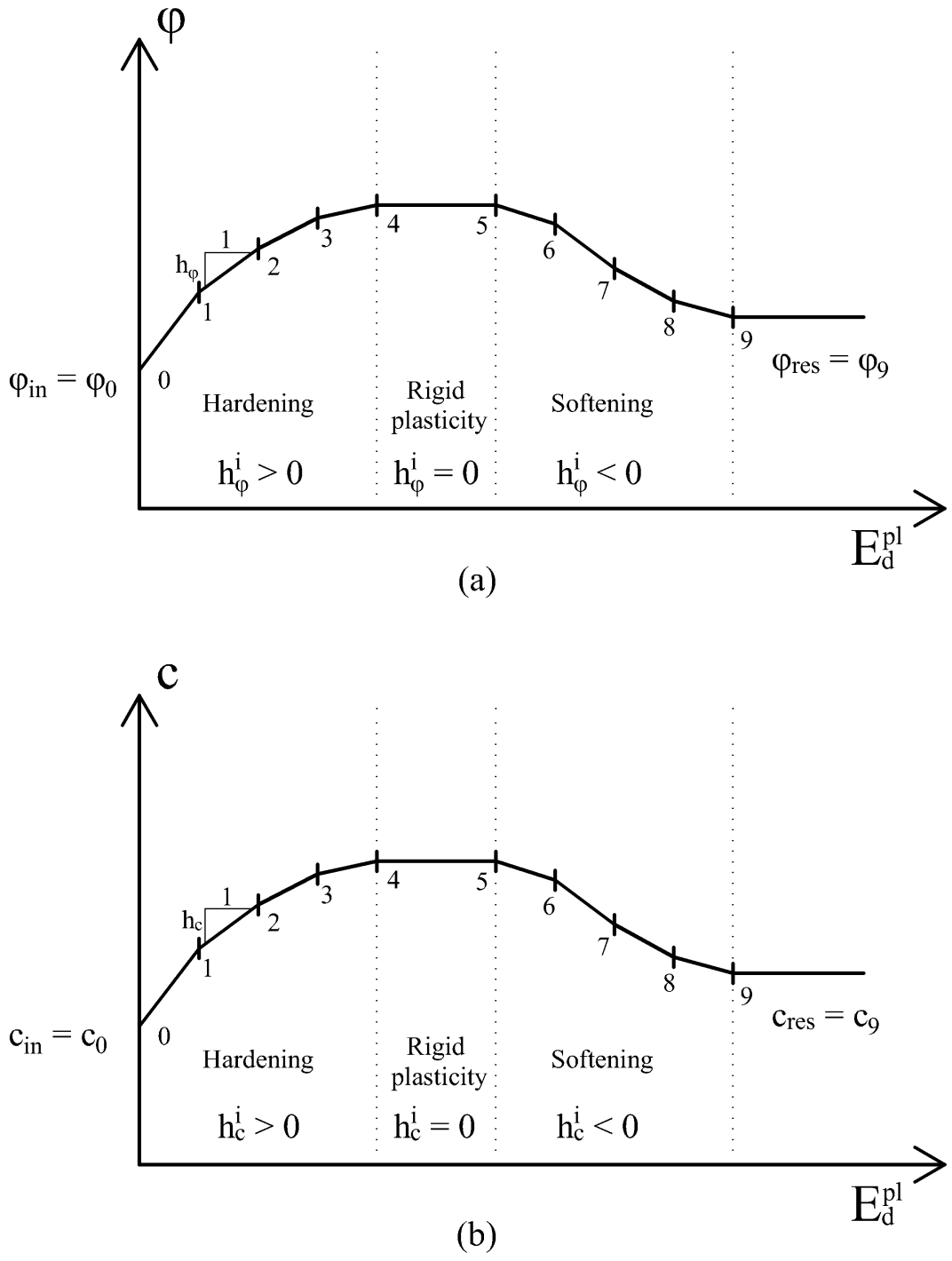

Figure 3.2: Hardening and softening modulus [17]: c_{in} and c_{res}, respective φ_{in} and φ_{res} represent initial and residual values of c and φ.

$$H = -\frac{\partial F}{\partial c}\frac{\mathrm{d}c}{\mathrm{d}E_d^{pl}}\frac{\mathrm{d}E_d^{pl}}{\mathrm{d}\lambda} - \frac{\partial F}{\partial \varphi}\frac{\mathrm{d}\varphi}{\mathrm{d}E_d^{pl}}\frac{\mathrm{d}E_d^{pl}}{\mathrm{d}\lambda}, \tag{3.15}$$

where

$$\frac{\partial F}{\partial \varphi} = \frac{c}{\sin^2\varphi}M_{JP} + (\sigma_m - c\cot\varphi)\frac{\mathrm{d}M_{JP}}{\mathrm{d}\varphi}, \tag{3.16}$$

$$\frac{\mathrm{d}F}{\mathrm{d}c} = -\cot\varphi M_{JP}, \tag{3.17}$$

$$\frac{\mathrm{d}c}{\mathrm{d}\kappa} = \frac{\mathrm{d}c}{\mathrm{d}E_d^{pl}} = h_c, \tag{3.18}$$

$$\frac{\mathrm{d}\varphi}{\mathrm{d}\kappa} = \frac{\mathrm{d}\varphi}{\mathrm{d}E_d^{pl}} = h_\varphi. \tag{3.19}$$

Derivations of M_{JP} with respect to φ for selected values of θ are

$$\frac{\mathrm{d}M_{JP}^{ins}}{\mathrm{d}\varphi} = \frac{3\sqrt{3}\cos\varphi}{(3+\sin^2\varphi)^{\frac{3}{2}}}, \tag{3.20}$$

$$\frac{\mathrm{d}M_{JP}^{\theta=-30^\circ}}{\mathrm{d}\varphi} = \frac{6\sqrt{3}\cos\varphi}{(1-\sin\varphi)^2}, \tag{3.21}$$

$$\frac{\mathrm{d}M_{JP}^{\theta=30^\circ}}{\mathrm{d}\varphi} = \frac{6\sqrt{3}\cos\varphi}{(1+\sin\varphi)^2}. \tag{3.22}$$

By accepting the strain hardening approach, we can write

$$\mathrm{d}\kappa = \mathrm{d}E_d^{pl} = \sqrt{2(\Delta e^{pl})^T\Delta e^{pl}} = \mathrm{d}\lambda \Rightarrow \frac{\mathrm{d}E_d^{pl}}{\mathrm{d}\lambda} = 1, \tag{3.23}$$

where Δe^{pl} stands for the increment of deviatoric plastic strain vector. With final substitution of Eq. (3.16)-(3.23) back into Eq. (3.15), result is searched form of the hardening/softening modulus as

$$H = h_c\cot\varphi M_{JP} - h_\varphi\left[\frac{c}{\sin^2\varphi}M_{JP} + (\sigma_m - c\cot\varphi)\frac{\mathrm{d}M_{JP}}{\mathrm{d}\varphi}\right]. \tag{3.24}$$

3.1.3 Cap formulation

The main modification of the Drucker-Prager model is compression cap. The formulation of the cap model was first proposed in 1989 in [15], but in this thesis the form presented in [17] is utilized. It is represented by variable F_c^c in Eq. 3.1 and Eq. 3.8 and changes

shape of the yield criterion with creating an elliptical hardening cap, as you can see in Fig 3.1. Dimensionless variable F_c^c is defined as

$$F_c^c(\sigma, X(\kappa_2), L(R, c(\kappa_1), \varphi(\kappa_1), X(\kappa_2))) = 1 - \frac{(\sigma_m + L)\left[(\sigma_m + L) - |\sigma_m + L|\right]}{2(X - L)^2}, \quad (3.25)$$

where X and L are the hardening cap parameters of the cap. They are related by

$$L = \frac{X - Rc\cot\varphi}{1 + R}, \quad (3.26)$$

where R is a material parameter that defines the ellipticity of the yield cap. Development of the cap hardening is assumed by κ_2, which is in our case the current volumetric plastic strain ε_v^{pl}. The κ_1 is still the deviatoric plastic strain E_d^{pl}. Hardening of the compressive cap is presented in [8] and is defined by

$$X = X_0 - \frac{1}{D}\ln\left(1 + \frac{\varepsilon_v^{pl}}{W}\right), \quad (3.27)$$

where X_0 is the initial abscissa intercept of the cap surface, W represents maximum volumetric plastic strain and D is shape factor. Note that L represents the absolute value of the mean effective stress at the point of interception of the two yield surfaces, f_d (Drucker-Prager surface) and f_c (Cap surface). This model assumes only hardening of the material in compression, so whenever $L < L_{max}(X_{max})$ we set $L = L_{max}$ to the maximum value of L reached.

3.1.4 Calculation procedure and implementation

Total stress can be calculated as

$$\sigma = \mathbf{D}^{el}\varepsilon_{el}, \quad (3.28)$$

where $\mathbf{D}^{el}$ is an ordinary isotropic stiffness matrix and ε_{el} is a elastic deformation vector. Calculation is performed in explicit software MARS finite element solver [9], so model is implemented in the incremental form. Then Eq. 3.28 is modified as

$$\sigma^{n+1} = \sigma^n + \mathbf{D}^{el}\mathrm{d}\varepsilon_{el}. \quad (3.29)$$

During numerical procedure, the trial stress $\sigma_{tr}^{n+1} = \sigma^n + \mathbf{D}^{el}\mathrm{d}\varepsilon$, where $\mathrm{d}\varepsilon$ is a strain increment, is calculated at the beginning of each step. If Eq. 3.1 is satisfied, strains and stresses are stored, and calculation continues with next deformation increment. If the yield function is violated, the material behavior changes from the basic elastic to the elasto-plastic with hardening. Due to higher amount of the variables, which describe

return to the yield surface of plasticity, it is necessary to implement the Jacobian matrix[5]. There are eight material parameters driving the return to yield surface of plasticity:

- $\Delta\lambda$ - Coefficient of plastic flow,
- c - Cohesion,
- φ - Angle of friction,
- ψ - Angle of dilatation,
- ξ - Plastic volumetric stress along hydrostatic axis,
- X - Abscissa intercept of the cap surface,
- L - Point of interception of the cap and Drucker-Prager surface,
- a_{pp} - Negative part of the plastic potential function.

Before describing the Jacobian matrix, we need to define basic equations, to be used for the definition of all variables. Assume that the plastic strain increment have the form

$$\mathrm{d}\varepsilon^{pl} = \Delta\lambda \frac{\partial G}{\partial \sigma}, \tag{3.30}$$

and with accepting this flow rule, increments of yield respective plastic strain has the form

$$\mathrm{d}\varepsilon_{\nu}^{pl} = \mathrm{d}\lambda \frac{\partial G}{\partial \sigma_m} = \Delta\lambda M_{JP}^{PP} \sin\psi, \tag{3.31}$$

$$\mathrm{d}E_{d}^{pl} = \mathrm{d}\lambda \frac{\partial G}{\partial J} = \Delta\lambda, \tag{3.32}$$

which further allows writing the corresponding stresses at the end of the $i+1$ load increment as

$$\sigma_m^{i+1} = \sigma_m^{tr} - \xi, \tag{3.33}$$

$$J^{i+1} = \frac{J^{tr}}{1 + 2\mu^i \delta\lambda} \Delta\lambda, \tag{3.34}$$

$$\Delta\varepsilon_v^{pl}(\xi) = \frac{\xi}{K^i}, \tag{3.35}$$

[5]Matrix of partial derivations

where K is the bulk modulus and μ represents the elastic shear modulus to avoid misinterpretation with the plastic potential function. Then the Jacobian matrix can be already defined.

- Primary variables of Jacobian matrix are

$$\{\mathbf{a}\}^T = \{\Delta\lambda, c^{i+1}, \sin\varphi^{i+1}, \sin\psi^{i+1}, \xi, X^{i+1}, L^{i+1}, a_{pp}^{i+1}\}. \tag{3.36}$$

- Residuals of the Jacobian matrix are

$$\{\mathbf{r}\}^T = \{\mathcal{F}, \mathcal{C}, \Phi, \Psi, \mathcal{S}, \mathcal{X}, \mathcal{L}, \mathcal{G}\}, \tag{3.37}$$

where

$$\mathcal{F} = (J^{i+1})^2 - \left\{\left[(\sigma_m^{tr} - \xi) - c^{i+1}\cot\varphi^{i+1}\right] M_{JP}(\varphi^{i+1})\right\}^2 F_c^c(\sigma_m^{i+1}(\xi), X^{i+1}, L^{i+1}) = 0, \tag{3.38}$$

$$\mathcal{C} = c^{i+1} - \widehat{c} = 0, \tag{3.39}$$

$$\Phi = \sin\varphi^{i+1} - \sin\hat{\varphi} = 0, \tag{3.40}$$

$$\Psi = \sin\psi^{i+1} - \sin\widehat{\psi} = 0, \tag{3.41}$$

$$\mathcal{S} = \xi - K^i\widehat{\Delta\varepsilon}_v^{pl}(\Delta\lambda, \sigma_m^{i+1}(\xi), X^{i+1}, L^{i+1}, a_{pp}^{i+1}) = 0, \tag{3.42}$$

$$\mathcal{X} = X^{i+1} - \widehat{X}((\varepsilon_v^{pl})^i + \Delta\varepsilon_v^{pl}(\xi)) = 0, \tag{3.43}$$

$$\mathcal{L} = L^{i+1} - \widehat{L} = 0, \tag{3.44}$$

$$\mathcal{G} = (J^{i+1})^2 - \left\{\left[(\sigma_m^{tr} - \xi) - a_{pp}^{i+1}\right] M_{JP}^{PP}(\sin\psi^{i+1})\right\}^2 F_c^c(\sigma_m^{i+1}(\xi, X^{i+1}L^{i+1})) = 0. \tag{3.45}$$

Variables $\hat{c}$ and $\hat{\varphi}$ follows Eq.(3.10) and (3.11) and the current value of dilatation angle $\hat{\psi}$ can be, with help of Rowe's dilatation theory in triaxial compression, written as

$$\sin\hat{\psi} = \frac{\sin\varphi^{i+1} - \sin\varphi_{cv}}{1 - \sin\varphi^{i+1}\sin\varphi_{cv}}, \tag{3.46}$$

where φ_{cv} is a constant-volume friction angle. Variable $\widehat{X}$ and $\widehat{L}$ are defined according Eq. 3.27, Eq. 3.26 respectively. Resulting incremental equations are

$$\widehat{X} = X_0 - \frac{1}{D} ln\left[1 + \frac{(\varepsilon_v^{pl})^i + \Delta\varepsilon_v^{pl}(\xi)}{W}\right], \tag{3.47}$$

$$\widehat{L} = \frac{X^{i+1} - Rc^{i+1}\cot\varphi^{i+1}}{1 + R}. \tag{3.48}$$

- Local Newton-Raphson method, which have the form

$$\{a^{i+1}\}_{k+1} = \{a_k^{i+1}\} - [\mathbf{H}]^{-1}\{r\}_k. \tag{3.49}$$

- Jacobian matrix $[\mathbf{H}]$

$$[\mathbf{H}] = \begin{bmatrix} \frac{\partial \mathcal{F}}{\partial \Delta\lambda} & \frac{\partial \mathcal{F}}{\partial c} & \frac{\partial \mathcal{F}}{\partial \sin\varphi} & 0 & \frac{\partial \mathcal{F}}{\partial \xi} & \frac{\partial \mathcal{F}}{\partial X} & \frac{\partial \mathcal{F}}{\partial L} & 0 \\ \frac{\partial \mathcal{C}}{\partial \Delta\lambda} & \frac{\partial \mathcal{C}}{\partial c} & 0 & 0 & 0 & 0 & 0 & 0 \\ \frac{\partial \Phi}{\partial \Delta\lambda} & 0 & \frac{\partial \Phi}{\partial \sin\varphi} & 0 & 0 & 0 & 0 & 0 \\ 0 & 0 & \frac{\partial \Psi}{\partial \sin\varphi} & \frac{\partial \Psi}{\partial \sin\psi} & 0 & 0 & 0 & 0 \\ \frac{\partial \mathcal{S}}{\partial \Delta\lambda} & 0 & 0 & \frac{\partial \mathcal{S}}{\partial \sin\psi} & \frac{\partial \mathcal{S}}{\partial \xi} & \frac{\partial \mathcal{S}}{\partial X} & \frac{\partial \mathcal{S}}{\partial L} & \frac{\partial \mathcal{S}}{\partial a_{pp}} \\ 0 & 0 & 0 & 0 & \frac{\partial \mathcal{X}}{\partial \xi} & \frac{\partial \mathcal{X}}{\partial X} & 0 & 0 \\ 0 & \frac{\partial \mathcal{L}}{\partial c} & \frac{\partial \mathcal{L}}{\partial \sin\varphi} & 0 & 0 & \frac{\partial \mathcal{L}}{\partial X} & \frac{\partial \mathcal{L}}{\partial L} & 0 \\ \frac{\partial \mathcal{G}}{\partial \Delta\lambda} & 0 & 0 & \frac{\partial \mathcal{G}}{\partial \sin\psi} & \frac{\partial \mathcal{G}}{\partial \xi} & \frac{\partial \mathcal{G}}{\partial X} & \frac{\partial \mathcal{G}}{\partial L} & \frac{\partial \mathcal{G}}{\partial a_{pp}} \end{bmatrix}. \tag{3.50}$$

- Initial conditions

$$\{a_0\}^T = \{0, c^i, \sin\varphi^i, \sin\psi^i\}, \tag{3.51}$$

$$\{r_0\}^T = \{J^{tr} + (\sigma_m^{tr} - c^i \cot\varphi^i) M_{JP}(\sin\varphi^i), 0, 0, 0\}. \tag{3.52}$$

3.1.5 Partitioning of algorithm

Such a large Jacobian matrix is complicated to compute. Also two possible scenarios can happen after exceeding the yield of plasticity, as you can see in Fig. 3.3. One possible scenario is *subcritial compression* and the second is *supercritical dilatation*. When we use single equation for the yield of plasticity, some difficulties can occur. For example returning from the subcritical region with zero dilatation angle. Secondly, when returning from supercritical dilation part with non-zero dilatation angle. For that reason, we divided returning to the yield of plasticity into the two main parts (simplest solution). These behaviors are separated by crossover point $\tilde{L}$, which is calculated from equation

$$\tilde{L} = \frac{(-3L + c\cot\varphi) - \sqrt{A}}{4}, \tag{3.53}$$

$$A = (-3L + c\cot\varphi)^2 - 8\left[L^2 - Lc\cot\varphi - (X - L)^2\right]. \tag{3.54}$$

This division of the yield criterion leads to decrease of variables needed for the returning algorithm.

- *Return from subcritical region*: In this region, we can use an associated flow rule by

assuming $\psi = \varphi$. Also we can ignore the possibility of modifying the shear strength parameters φ and c. This give us set of residuals

$$r = \{\mathcal{F}, \mathcal{S}, \mathcal{X}, \mathcal{L}\}^T . \tag{3.55}$$

- *Return from region of supercritical dilatation*: When exceeding yield surface on this side, the plasticity equation cannot increase volumetric plastic strain. Assuming this fact, we can skip variables X and L. This leads to set of residuals

$$r = \{\mathcal{F}, \mathcal{S}, \mathcal{C}, \Phi, \Psi, \mathcal{G}\}^T . \tag{3.56}$$

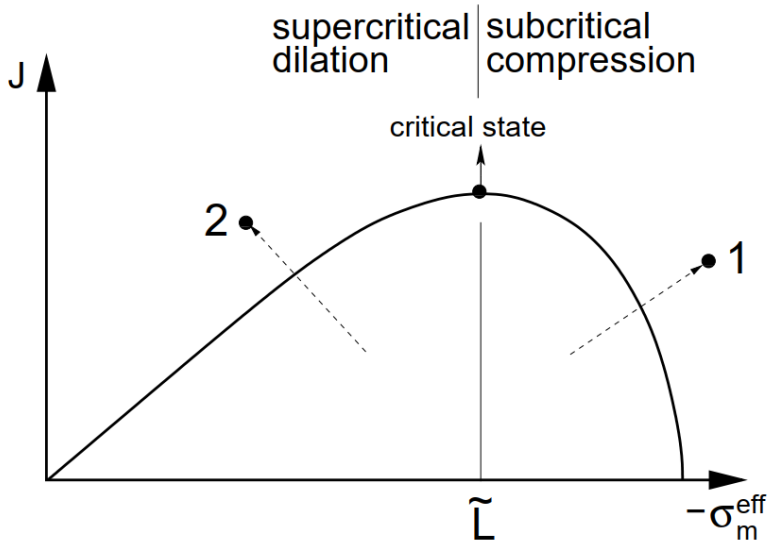

Figure 3.3: Returning scenarios after exceeding yield of plasticity. [17].

3.1.6 Apex problem

Two cones are shown in Fig. 3.4. The first cone K_ε (following direction of the plastic strain vector), shows inadmissible region for the plastic strain increment. The second cone K_σ shows the admissible stress domain. If the stress point is located in a region K_σ, material behavior is elastic, if it is located outside of K_σ but also outside of K_ε, the computation performs regular stress return. However, if the stress point is located inside the K_ε cone, the stress update is simply a return mapping to the apex. That situation may occur in two cases: (a) right after load increment, but also (b) when performing regular stress return, due to changing of material parameters. Such a situation can be called as an "apex problem".

$$\dot{\varepsilon}_v \geq M_{JP}^{PP} \dot{E}_d^{pl}. \tag{3.57}$$

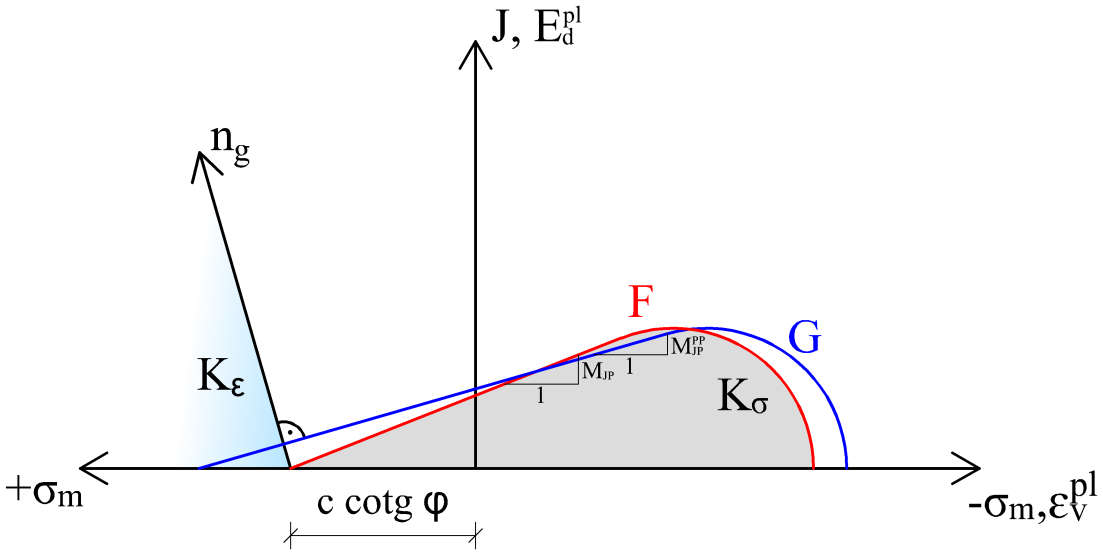

Figure 3.4: Apex admissible regions for stresses and plastic strain rates [17].

In the literature we can find two different stands for performing apex problem:

- Return with constant material parameters.
- Return with hardening/softening material.

At the first case, stress point just return to the apex (Fig.3.4), so stress takes the form

$$\sigma^{i+1} = 3c^i \cot \varphi^i \mathbf{m}. \tag{3.58}$$

If the second approach is chosen, we can use two facts. The first is that material parameters c and φ are functions of the deviatoric plastic strain E_d^{pl}. The second is that when returning to the apex point, elastic strain has only volumetric part so ΔE_d^{pl} can be determined at first, because it does not change. And if elastic strain has only volumetric part, deviatoric plastic strain vector is equal to the deviatoric increment strain vector. Then $\mathrm{d}E_d^{pl}$ can be determined by the deviatoric strain measure, which has the form

$$\Delta E_d^{pl} = \sqrt{2\Delta e_{ij}^{pl} \Delta e_{ij}^{pl}}, \tag{3.59}$$

where e^{pl} represents deviatoric plastic strain vector. As next, hardening of parameters c and φ follows Eqs. (3.10) and (3.11) with current E_d^{pl}. Then the stress takes the form with updated c and φ, similar to Eq. (3.58), as

$$\sigma^{i+1} = 3c^{i+1}\cot\varphi^{i+1}\mathbf{m}. \tag{3.60}$$

In both cases, variables X and L remains unchanged.

3.1.7 Isotropic compression

When an element is compressed along the hydrostatic axis and $J \to 0$, the system of residuals is reduced to

$$r = \begin{Bmatrix} \mathcal{F} \\ \mathcal{X} \end{Bmatrix} = \begin{Bmatrix} \sigma_m^{i+1} + X^{i+1} \\ X^{i+1} - \widehat{X} \end{Bmatrix} = \begin{Bmatrix} 0 \\ 0 \end{Bmatrix}, \tag{3.61}$$

with two unknowns $a = \{X^{i+1}, \sigma_m^{i+1}\}^T$. The $\widehat{X}$ follows Eq. 3.47. Equivalently with the apex problem, the increment of the volumetric plastic strain has form

$$\Delta\varepsilon_v^{pl} = \frac{\sigma_m^i + K^i\Delta\varepsilon_v - \sigma_m^{i+1}}{K^i}. \tag{3.62}$$

Then the Jacobian matrix has form

$$H = \begin{bmatrix} \frac{\partial\mathcal{F}}{\partial X} & \frac{\partial\mathcal{F}}{\partial\sigma_m} \\ \frac{\partial\mathcal{X}}{\partial X} & \frac{\partial\mathcal{X}}{\partial\sigma_m} = -\frac{\partial\widehat{\mathcal{X}}}{\partial\Delta\varepsilon_v^{pl}}\frac{\partial\Delta\varepsilon_v^{pl}}{\partial\sigma_m} \end{bmatrix} = \begin{bmatrix} 1 & 1 \\ 1 & H_{22} \end{bmatrix}, \tag{3.63}$$

where the H_{22} is given by

$$H_{22} = -\frac{1}{D\left[W + (\varepsilon_v^{pl})^i + \Delta\varepsilon_v^{pl}\right]}\frac{1}{K^i}. \tag{3.64}$$

3.2 Kelvin Chain

As you can see in 1.3.4, the Kelvin reological model is simple mechanical model for simulating viscoelastic behavior. In this thesis Kelvin chain description is inspired by [18]. Kelvin-Voigt reological model consists of a dashpot and linear spring, which are connected in parallel as you can see in Fig. 3.5. Under constant total stress σ_0 applied at time $t_0 = 0$, the strain ε in the Kelvin model is given by

$$\varepsilon = \frac{\sigma_0}{E_\eta}(1 - e^{-E_\eta t/\eta}), \tag{3.65}$$

where E_η is the spring stiffness and η represents viscous damping of the dashpot. The

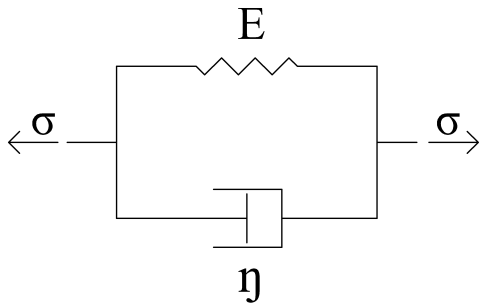

Figure 3.5: Detail of the Kelvin-Voigt model. [18].

Kelvin-Voigt model itself does not manage instantaneous elastic strain during the application or removal of the stress. The strain will converge asymptotically to the potential maximum σ_0/K, when total stress will be hold only with linear spring. Constant η/E, with units of time, is known as te retardation time λ_η of the Kelvin element. If a constant stress σ_0 is 1 and is applied at time τ, then the Eq. 3.65 can be used to describe the compliance function of the Kelvin model. This function has the form

$$\varepsilon = \sigma_0 J(t,\tau) = \sigma_0 \left\{ \frac{1}{E_\eta} \left[1 - e^{-(t-\tau)/\lambda_\eta} \right] \right\}. \tag{3.66}$$

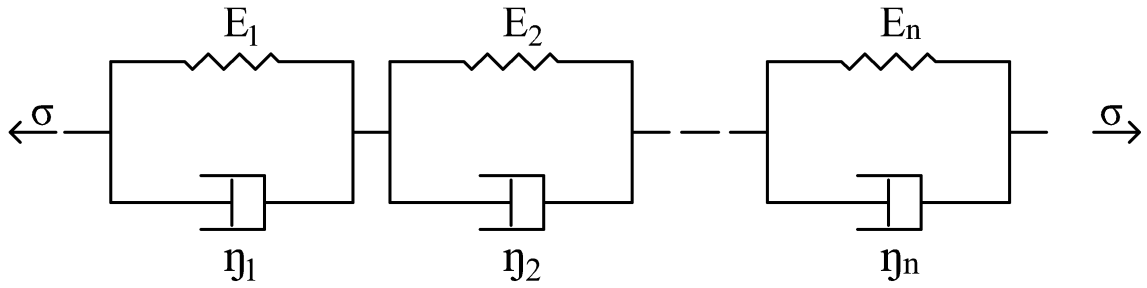

Figure 3.6: Kelvin chain created by individual Kelvin-Voigt elements. [18].

If the applied stress is not constant, and assuming the Boltzmann superposition principle holds, the convolution between the changing stress rate $\partial\sigma(\tau)/\partial\tau$ and the compliance function $J(t,\tau)$ must be considered

$$\varepsilon(t) = \int_0^t J(t,\tau) \frac{\partial\sigma(\tau)}{\partial\tau} d\tau. \tag{3.67}$$

The Kelvin chain model for viscoelastic behavior is set of Kelvin models connected in series, as you can see in Fig. 3.6. Each Kelvin element in the series is loaded with the same total stress. Then the total strain is the summation of the strain from each individual Kelvin element. For constant stress σ_0 applied at time t_0, then the Kelvin chain model can be written as a Dirichlet series

$$\varepsilon(t) = \sigma_0 J(t,\tau) = \sigma_0 \sum_{i=1}^{n} \frac{1}{E_{\eta,i}} (1 - e^{-(t-\tau)/\lambda_{\eta,i}}). \tag{3.68}$$

3.3 Calculation algorithm

The Kelvin chain model is connected to the Drucker-Prager model serially. The Drucker-Prager model represents elasto-plastic behavior of material. The resulting strains and stresses along with time step Δt are used for the calculation of creep or relaxation strains with Kelvin chain model. Our implementation is used in an explicit solver, which is not optimal for simulating creep and relaxation. However, the solver allows time mapping, which helps to describe the material behavior over time.

The algorithm used for the calculation is:

1. At the beginning of the simulation, the input file is loaded. Then the solver will initialize and create a sample model, create a mesh composed of elements, and appropriate material for each element is assigned.

2. The strain increment occurs.

3. From the known total strain ε, eigen strain ε_{eig} and plastic strain ε_{pl} values, the elastic stress σ_e is calculated, followed by the first, respective the second stress invariant evaluation. Then a decision is proceed whether the stress in the element did not exceed the yield criterion. If the criterion is exceeded, the algorithm of return to the yield surface is executed, following point 4. If the criterion is not exceeded, the material behaves elastically and the algorithm proceeds to point 5.

4. The algorithm decides where the yield criterion was exceeded. According to the location the type of return to the yield criterion is decided. The selected part calculates return to the yield criterion. The calculated results are stresses and plastic strains.

5. The eigen strain ε_{eig} is calculated from the current state of the element.

6. The last part of the cycle, storing all state variables that were changed. The current elastic stresses, total, plastic and eigen strains are also stored. Then the calculation continues in the point 2 with another increment of strains.

4 Results

This chapter is focused on the results of our work. In the chapter 3, the utilized approach for the simulation of thermoset polymers behavior is described .The approach includes elastic, plastic and viscous responses to the loading. For the elastoplastic part we implemented Drucker-Prager yield criterion with compression cap. Results of the elastoplastic behavior are presented in the first part of this chapter. The second part is focused on the results of simulating viscous behavior of material. This type of response is created by serially connecting the Drucker-Prager model to the Kelvin chain. These numerical approaches were newly implemented into the MARS finite element solver [9]. Kelvin chain was implemented before, but link with the Drucker-Prager model was newly added.

4.1 Drucker-Prager results

To verify Drucker-Prager model we utilized the compression test, where the cap has the greatest impact. We decided for the same test, which we utilized in my bachelor thesis. This simple compression test of the vinyl-ester mortar was proposed in [20]. As you can see in the scheme in Fig. 4.1, specimen is beam with width and height 24 mm and length 74 mm. The specimen is settled between two solid plates, rigidly on the bottom and with the possibility of movement on the top. Top plate is fixed in all horizontal directions but can rotate around horizontal axes. Bottom plate is fixed in all directions and rotations as well. The load on the element is generated with moving the upper part of apparatus to the bottom, while displacement and force are recorded.

The model of the test sample, as shown in Fig. 4.2, is divided by height into 18 layers, each containing 108 elements. All together, the model consists of 1944 elements. The size of the element is about 4 mm. Elements with a single integration point were used to calibrate the calculations, which accelerated the calculation speed. Finally, elements containing eight integration points were used for the final results. The final simulation is more time-consuming, but the results are more accurate. The top and bottom plates are identical, and both are modeled as rigid bodies.

In Fig. 4.3 you can see experimental data as dashed red line. Next six lines represent different Drucker-Prager model configurations. Five of them were presented in my bachelor thesis [21]. Material parameters were used the same as in [20]: $E = 6792$ MPa; $\nu = 0.3$ at 25°C. Red, orange and purple lines represent results from Drucker-Prager model without hardening, also we employed associated flow-rule, i.e. $\phi = \psi$. Differences between these three lines are in the type of fitting to the Mohr-Coulomb yield criterion used in [20], because we used same parameters for our models. The first, dark blue line, is matching the Mohr-Coulomb in the triaxial compression, using Eq. 3.4. The second,

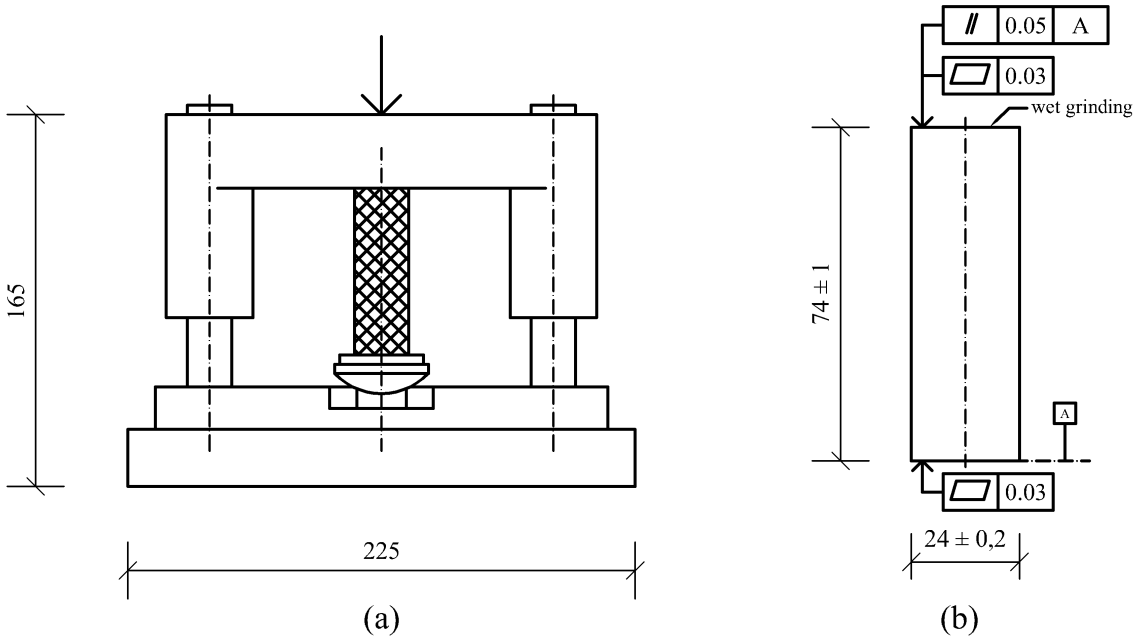

Figure 4.1: Compression test parameters: a) apparatus setup; b) specimen dimensions. [20, 21]

red line, is fitting the MC in the triaxial tension, using Eq. 3.5. The third, orange line, is matching MC model with inscribed cone using Eq. 3.6. Next two lines, which were presented in my bachelor thesis, are plotted in Fig. 4.3 as purple and green lines. Both are representing Drucker-Prager model with the evolution of the cohesion c. Purple line represents evolution defined by $c = 20$MPa for $E_d^{pl} = 0$ and $c = 40$MPa for the $E_d^{pl} = 0.05$. The green line stands for updated evolution characterized by $c = 15$MPa for $W_d^{pl} = 0$ and $c = 60$MPa for $E_d^{pl} = 0.15$. This update helped to better match of the experimental data. The last line, light blue, is representing Drucker-Prager model with cap. Material parameters are presented in Tab. 1. They differ a bit from [20], because our implementation of DP model with cap is different. As you can see in Fig. 4.3, the Drucker-Prager model with cap matches experimental data better, than models without compression hardening. However more additional experimental data are needed to properly characterize the model suitability for studied thermoset polymers.

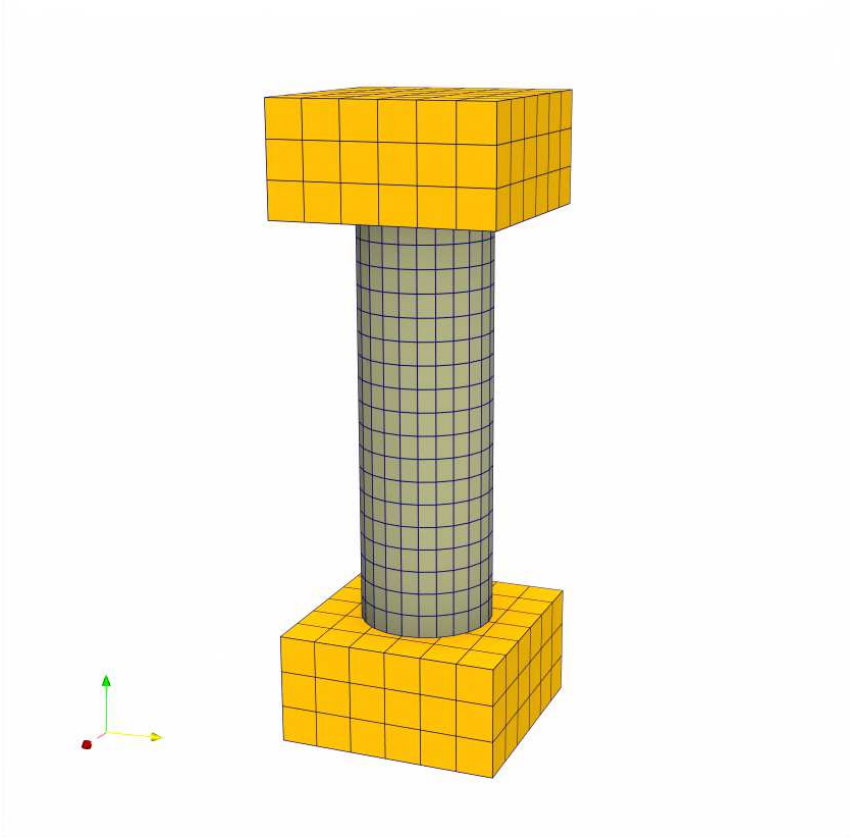

Figure 4.2: Model of test specimen used for simulation.

E	6.792 GPa
ν	0.3
c	35 MPa
φ	33°
ψ	26°
X_0	13 MPa
D	0.0026 MPa^{-1}
W	0.045
R	2.5

Table 1: Material parameters used for simulation of the Drucker-Prager model with cap.

4.2 Kelvin chain results

For the verification of the connection Drucker-Prager model with cap to the Kelvin chain, we decided to simulate the test as in previous section, but with some differences. Loading of the beam, as you can see in Fig. 4.4, was performed for approximately fifty minutes, then strain remains constant.

Our Kelvin chain parameters are presented in Tab. 2 and were taken from [18]. We

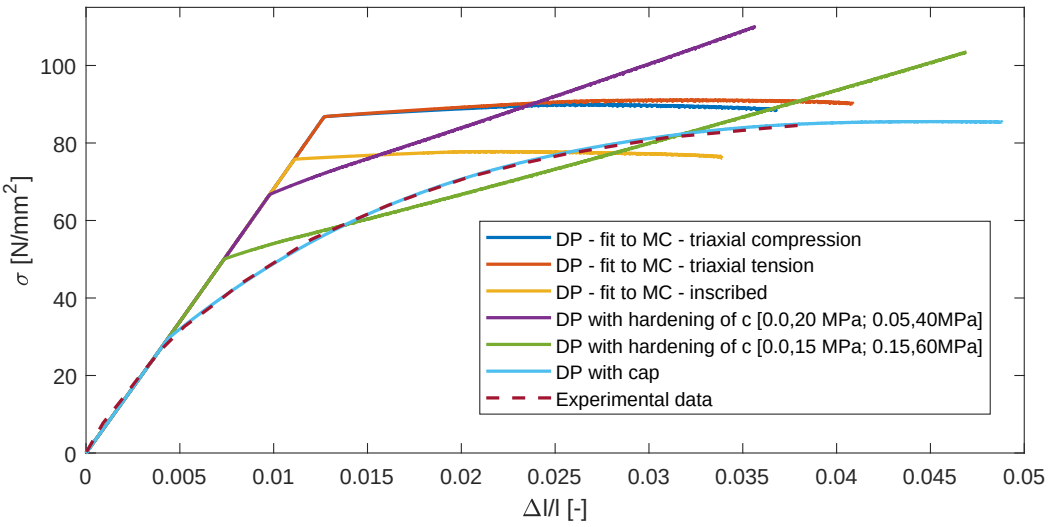

Figure 4.3: Compression tests compared real specimen results [20] and results from [21].

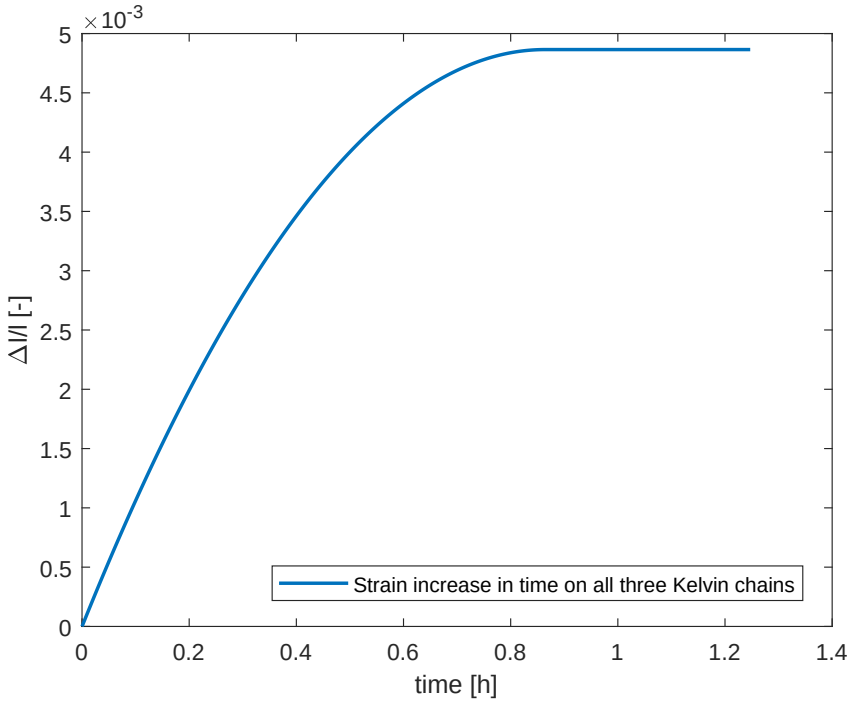

Figure 4.4: Loading progress during compression tests - strain-time diagram.

used calibration of the Drucker-Prager model with cap from Tab. 1. In Fig. 4.5, we can see stress-strain diagrams from our simulation. Blue line represents material cured for two days, red line shows material cured for three days and last yellow line is most cured material for seven days. As expected, with longer curing time, the strength of the material increases, indicating a gradient of stress increase.

$t_{0,i}$ [days]	$E_\lambda(t_{0,i})$ [MPa]					
	$\tau_1 = 0.001$ d	$\tau_2 = 0.01$ d	$\tau_3 = 0.1$ d	$\tau_4 = 1$ d	$\tau_5 = 10$ d	$\tau_6 = 100$ d
2	9.994e+04	1.933e+13	4.754e+03	1.755e+04	3.965e+04	3.721e+04
3	1.106e+04	1.924e+13	6.839e+04	1.812e+04	3.706e+04	3.370e+04
7	1.724e+04	2.361e+13	1.920e+04	2.415e+04	3.948e+04	3.343e+04

Table 2: Estimated moduli of the used Kelvin chains. Taken from Tab. 7. from [18].

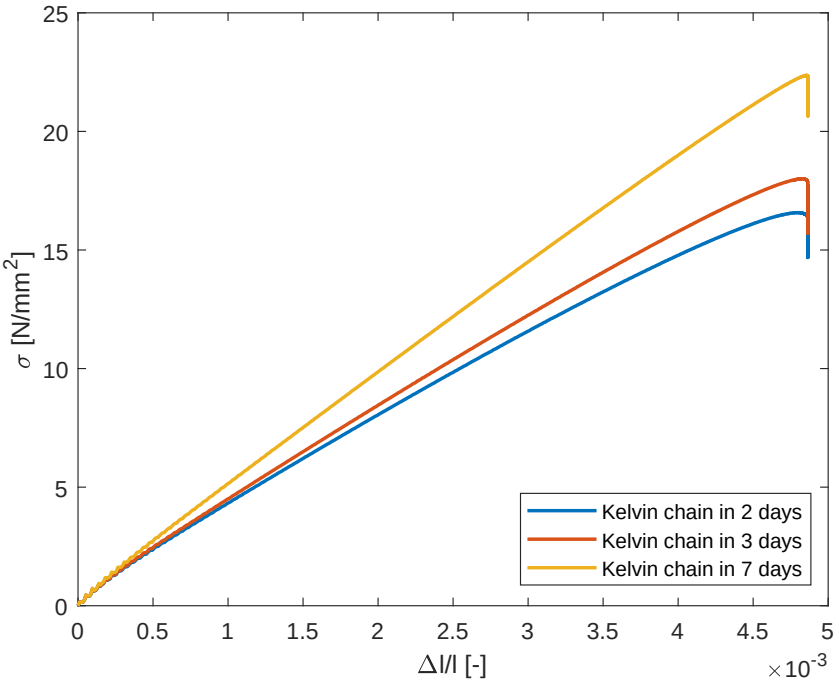

Figure 4.5: Compression tests of the beam stress-strain diagrams of the different Kelvin chains.

In Fig. 4.6 you can see stress-time diagram where the effect of relaxation is depicted. With longer curing time, the relaxation rate of the material also decreases and therefore the stress drop with time is slower.

As another test for the verification of the Kelvin model, we simulated a test where one Kelvin chain (in our case on the 7th day from Tab. 2) was loaded with the same deformation but at different times. Fig. 4.7 shows different load curves for each time. The blue curve represents the load after 1.71 hours, the red curve represents the load after 0.85 hours and the yellow curve represents the load after 0.2 hours.

Fig. 4.8 shows the different evolution of stresses at different loading times. The blue line represents the simulation with the lowest loading rate. The influence of relaxation is most visible here and the increase in stress during loading is the slowest. The red curve shows a simulation where the loading rate is higher than for the blue line, resulting in less

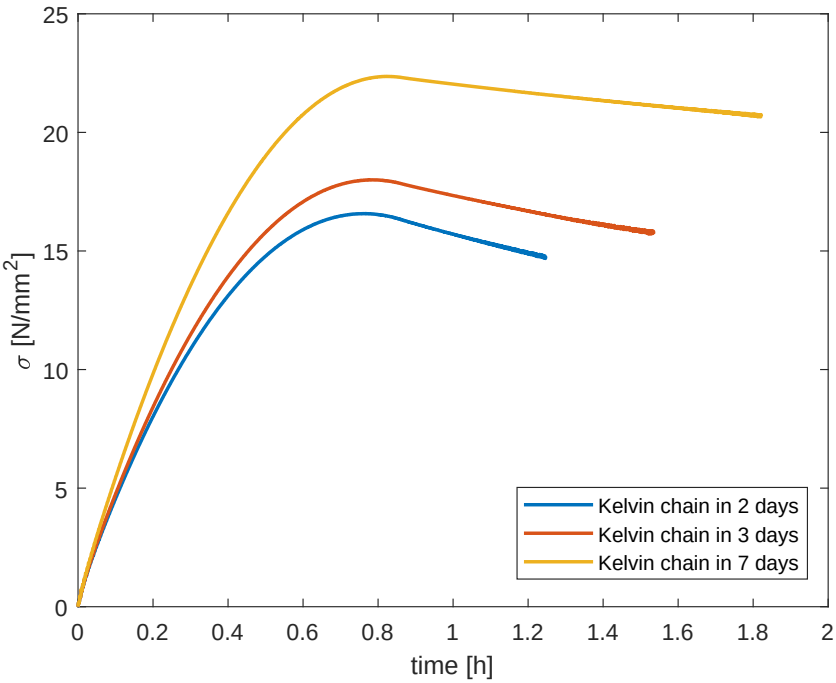

Figure 4.6: Compression tests of the beam stress-time diagrams with different Kelvin chains.

relaxation effect. The last, yellow line represents the simulation, when the loading time is the shortest, therefore there is a clearest influence of relaxation.

Fig. 4.9 shows the different stress evolution curves over time. The blue line, which represents the simulation with the longest loading time, has the lowest peak and is the smoothest of the curves, which is caused by the greatest material relaxation. The red curve shows the material response to the mean loading time. The yellow curve, which represents the simulation with the shortest loading time, has the steepest rise, the highest and the sharpest peak, because there is the least influence of creep during initial loading. Furthermore, it can be noted that the stress-decreasing trend due to material relaxation has a similar trend for all curves. This is due to the use of the same Kelvin chain.

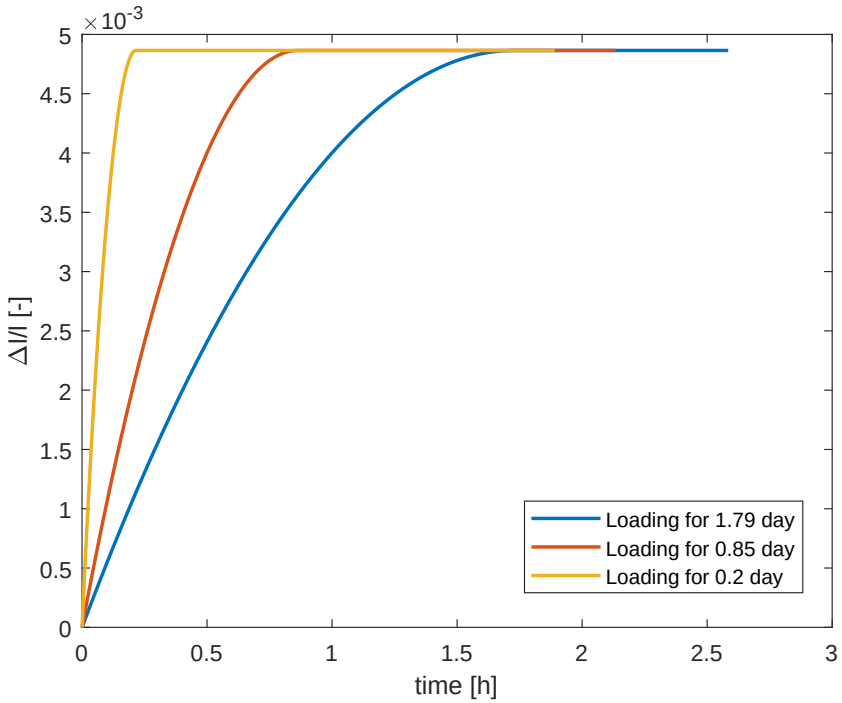

Figure 4.7: Influence of different loading speed on strain development during compression tests of one Kelvin chain.

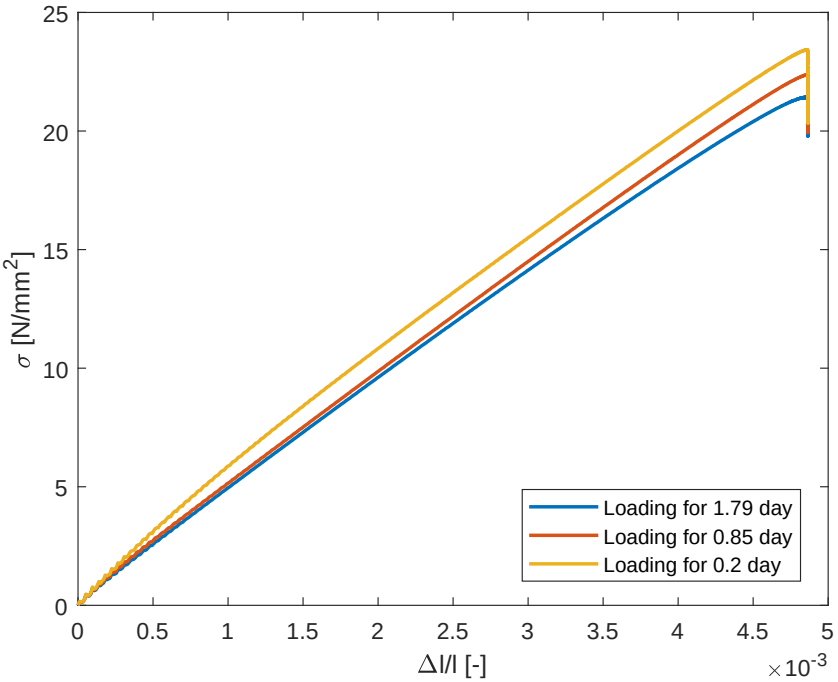

Figure 4.8: Influence of different loading speed on the stress-strain diagrams during compression tests of one Kelvin chain.

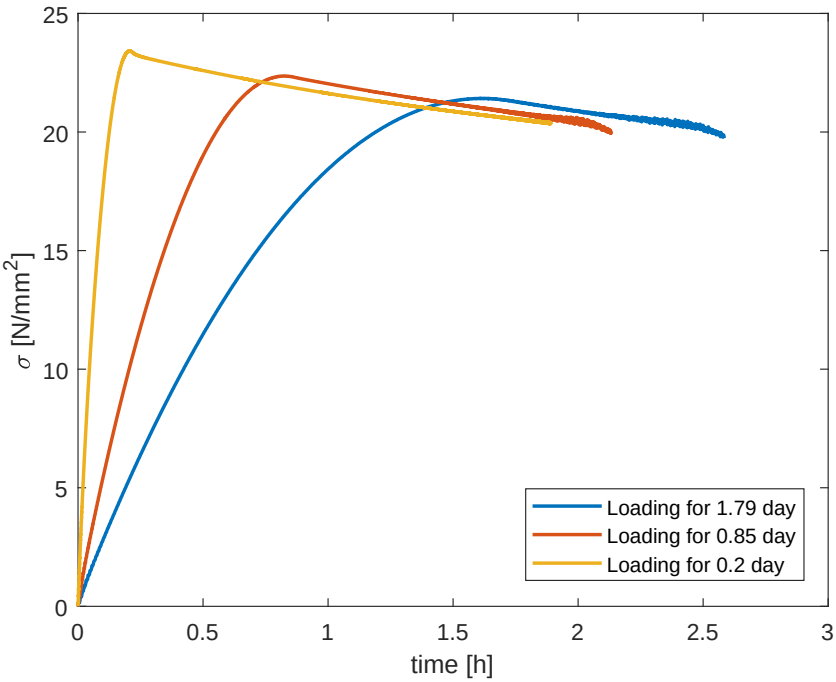

Figure 4.9: Influence of different loading speed on the stress progress during compression tests of one Kelvin chain.

5 Conclusion and future work

The main aim of this work was to describe and implement a model that will be able to simulate with sufficient accuracy the behavior of thermoset polymers under mechanical loading.

Improved Drucker-Prager cap model has been implemented in the MARS FEM solver. This model is able to more accurately describe the behavior of thermosetting plastics thanks to hardening in the compression. Furthermore, its binding to the Kelvin chain was added. This connection creates the model, that is able to simulate the creep effects over time. The preliminary results of the proposed model show that the behavior of the thermoset polymers over time is expected to be greatly influenced by creep effects.

Although the results of our work have improved the description of thermosets in the field of elasto-plastic behavior, the simulations of time dependent behavior are computationally demanding. Further, it would be appropriate to perform other simulations that would confirm the model's ability to simulate the behavior of thermosetting plastics in different loading scenarios.

The next step to improve the description of thermosets, their response to mechanical loading and parameter development is to use a more complex model, such as the Microplane M4 model described [7], in combination with a free volume approach proposed in [16]. This approach would allow to capture the effect of temperature and humidity on material behavior. These improvements are expected in further work.

References

[1] Traditional materials science tetrahedron. URL https://www.e-education.psu.edu/matse81/node/2094. Online [10/11/2019].

[2] Creep strains prorogres during time. URL https://www.thestructuralworld.com/2018/10/21/creep-shrinkage-explained/. Online [19/10/2019].

[3] The origins of the word matter. URL https://www.etymonline.com/word/matter. Online [07/12/2019].

[4] Annalingam Anandarajah. *Computational methods in elasticity and plasticity: solids and porous media*. Springer Science & Business Media, 2011.

[5] Ted L Anderson. Fracture mechanics-fundamentals and applications. *NASA STI/Recon Technical Report A*, 92, 1991.

[6] Eduardo A de Souza Neto, Djordje Peric, and David RJ Owen. *Computational methods for plasticity: theory and applications*. John Wiley & Sons, 2011.

[7] Giovanni Di Luzio. A symmetric over-nonlocal microplane model m4 for fracture in concrete. *International journal of solids and structures*, 44(13):4418–4441, 2007.

[8] Frank L DiMaggio and Ivan S Sandler. Material model for granular soils. *Journal of Engineering Mechanics*, 1971.

[9] ES3. Mars - modeling and analysis of the response structures. URL http://mars.es3inc.com/www_es3inc_com/marssolver/.

[10] Thomas JR Hughes. *The finite element method: linear static and dynamic finite element analysis*. Courier Corporation, 2012.

[11] He Liu, Hannele K. Zubeck, and Daniel H. Schubert. Finite-element analysis of helical piers in frozen ground. *Journal of Cold Regions Engineering*, 21(3):92–106, sep 2007. doi: 10.1061/(asce)0887-381x(2007)21:3(92).

[12] Marc André Meyers and Krishan Kumar Chawla. *Mechanical Behavior of Materials*. Cambridge University Press, 2 edition, 2008. ISBN 13 978-0-511-45557-5.

[13] Benoît Pardoen, Severine Levasseur, and Frédéric Collin. Using local second gradient model and shear strain localisation to model the excavation damaged zone in unsaturated claystone. *Rock Mechanics and Rock Engineering*, 48, 03 2014. doi: 10.1007/s00603-014-0580-2.

[14] Jean-Pierre Pascault, Henry Sautereau, Jacques Verdu, and Roberto JJ Williams. *Thermosetting polymers*, volume 64. CRC Press, 2002. ISBN 0-203-90840-6.

[15] D Pelessone. A modified formulation of the cap model. *Gulf Atomics Report GA-C19579 to the Defense Nuclear Agency*, 1989.

[16] Carl Frank Popelar and KM Liechti. Multiaxial nonlinear viscoelastic characterization and modeling of a structural adhesive. *Journal of Engineering Materials and Technology*, 119(3):205–210, 1997.

[17] Michal Sejnoha. *GEO FEM - Theoretical manual*. FINE Ltd., 2009.

[18] Patrícia Silva, Tiago Valente, Miguel Azenha, José Sena-Cruz, and Joaquim Barros. Viscoelastic response of an epoxy adhesive for construction since its early ages: Experiments and modelling. *Composites Part B: Engineering*, 116:266–277, 2017.

[19] Ferdinand Stoeckhert. *Fracture mechanics applied to hydraulic fracturing in laboratory experiments*. PhD thesis, 06 2015.

[20] Roland Unterweger. *Experimentelle und numerische Untersuchungen zum Tragverhalten von chemischen Verankerungen*. PhD thesis, University of Natural Resources and Life Sciences, Vienna, 1999.

[21] Jan Vozáb. Computational modeling of thermoset polymers with application to anchors, 2018.

[22] Olek C Zienkiewicz, Robert L Taylor, and Jian Z Zhu. *The finite element method: its basis and fundamentals*. Elsevier, 2005.